Cellular/Molecular

Fibroblastic SMOC2 Suppresses Mechanical Nociception by Inhibiting Coupled Activation of Primary Sensory Neurons

Shuo Zhang,[1,2,3] **Bing Cai,**[3,4] **Zhen Li,**[3] **Kaikai Wang,**[1,2,3] **Lan Bao,**[2,5] **Changlin Li,**[3,4,6] **and Xu Zhang**[1,2,3,4]

[1]Institute of Neuroscience and State Key Laboratory of Neuroscience, Center for Excellence in Brain Science and Intelligence Technology, University of Chinese Academy of Sciences, Chinese Academy of Sciences, Shanghai, 200031, China, [2]School of Life Science and Technology, ShanghaiTech University, Shanghai, 201210, China, [3]Research Unit of Pain Medicine, Chinese Academy of Medical Sciences; and SIMR Joint Lab of Drug Innovation, Shanghai Advanced Research Institute, Chinese Academy of Sciences; Shanghai Research Center for Brain Science and Brain-Inspired Intelligence, Shanghai, 201210, China, [4]Guangdong Institute of Intelligence Science and Technology, Hengqin, Zhuhai, 519031, China, [5]State Key Laboratory of Cell Biology, Shanghai Institute of Biochemistry and Cell Biology, Center for Excellence in Molecular Cell Science, Chinese Academy of Sciences, Shanghai, 200031, China, and [6]Department of Pain Medicine and Shenzhen Municipal Key Laboratory for Pain Medicine, Huazhong University of Science and Technology Union Shenzhen Hospital, Shenzhen, 518060, China

Nociceptive information is detected and transmitted by neurons in the DRG. Recently, single-cell RNA sequencing has revealed the molecular profile of various cell types, including fibroblasts in the DRG. However, the role of molecules in fibroblasts needs to be elucidated in nociceptive regulation. Here, we found that secreted modular calcium-binding protein 2 (SMOC2) was secreted by fibroblasts to become a component of basement membrane and envelop the unit consisting of DRG neurons and attached satellite glial cells. KO of *Smoc2* in both sexes of mice led to increased neuronal clusters and decreased mechanical threshold, but unchanged noxious thermal response. Knockdown of *Smoc2* in the DRG phenocopied the behavioral performance by *Smoc2* KO in both sexes of mice. *In vivo* calcium imaging showed that *Smoc2* KO increased coupled activation of adjacent DRG neurons induced by nociceptive mechanical stimuli, which was reversed by DRG injection of SMOC2. Importantly, SMOC2 interacted with P2X7 receptor (P2X7R) and suppressed ATP-induced activation in HEK293 cells expressing this receptor. Injection of A740003, an antagonist of P2X7R, to the DRG reduced coupled activation of adjacent DRG neurons induced by nociceptive mechanical stimuli but did not further enhance the SMOC2-inhibited effect. Furthermore, peripheral inflammation resulted in a decreased SMOC2 and increased neuronal clusters. DRG injection of SMOC2 inhibited the neuronal coupling resulted from peripheral inflammation. This study reveals a specific role of fibroblastic SMOC2 in suppressing mechanical nociception through inhibiting the communication of adjacent DRG neurons, which provides an important mechanism of fibroblasts in nociceptive regulation.

Key words: **DRG; fibroblast; mechanical nociception; SMOC2**

Significance Statement

The function of fibroblastic molecules is rarely noticed in the regulation of nociceptive sensation. Here, we reveal that fibroblastic SMOC2 is secreted to be a component of basement membrane and surrounded the unit consisting of DRG neuron and attached satellite glial cells. SMOC2 is required for maintaining the basal mechanical nociceptive threshold in the DRG. Loss of SMOC2 leads to the increased coupled activation of adjacent DRG neurons induced by noxious mechanical stimuli. Peripheral inflammation causes decreased fibroblast cells and SMOC2, which may result in the increase of coupled activation of adjacent DRG neurons. Mechanistically, SMOC2 interacts with and suppresses satellite glial P2X7 receptor to inhibit the coupled activation of adjacent DRG neurons.

Received Oct. 26, 2021; revised Apr. 3, 2022; accepted Apr. 6, 2022.

Author contributions: X.Z., S.Z., C.L., and L.B. designed research; S.Z., L.B., C.L., and X.Z. wrote the paper; S.Z., B.C., Z.L., and K.W. performed research; S.Z., B.C., Z.L., and K.W. analyzed data.

This work was supported by National Natural Science Foundation of China 32071001, 32192413, 31671094, and 32030050; Chinese Academy of Sciences QYZDYSSW-SMC007; Special Fund for Science-Technology Innovation Strategy of Guangdong Province 2021B0909050004; Science and Technology Commission of Shanghai Municipality 18JC1420301; Innovation Fund for Medical Sciences of Chinese Academy of Medical Sciences 2019-I2M-5-082; and Shenzhen Sanming Project.

The authors declare no competing financial interests.

Correspondence should be addressed to Xu Zhang at zhangx@sari.ac.cn or Changlin Li at licl@gdiist.cn.

https://doi.org/10.1523/JNEUROSCI.2132-21.2022

Introduction

DRG receives the information of various stimuli from external environment. The major cell types with known functions in the DRG are neurons, satellite glia cells (SGCs), and Schwann cells. DRG neurons are pseudo-unipolar neurons that send one branch to the periphery and the other to the spinal cord, which detect and transmit somatosensory information to the CNS (Hanani, 2005; Basbaum et al., 2009). Small-diameter DRG neurons and medium-diameter DRG neurons are traditionally considered to be related to nociceptive transmission, and large-

diameter DRG neurons detect innocuous mechanical stimulation. SGCs are specialized glia cells in the PNS, and play important roles in nourishing DRG neurons and regulating somatosensory sensation (Hanani, 2015; Fan et al., 2019). Schwann cells are also myelinating glial cells of the PNS wrapped around the nerve fibers to accelerate the transmission of electrical signal and participate in the process of axonal regeneration of DRG neurons after injury (Scherer and Arroyo, 2002; Bolivar et al., 2020). Most DRG neurons cannot directly contact with each other because of the tightly enveloping of SGCs (Huang et al., 2013; Hanani, 2015). Therefore, the communication of adjacent DRG neurons is mediated by the attached SGCs (Huang et al., 2013). Increased coupled activation of adjacent DRG neurons through SGCs contributes to nociceptive hypersensitivity under pathologic conditions (Hanani, 2015; Kim et al., 2016).

Recent studies report that various cell types, especially fibroblasts, other than neurons and glia cells are contained in the DRG (Wang et al., 2021). Fibroblasts are the most common cells of connective tissues with limited specific markers to define their population (Kirk et al., 2021). Fibroblasts synthesize and secrete proteins to form the extracellular matrix of connective tissue and maintain structural integrity (Parsonage et al., 2003; Lynch and Watt, 2018). In the CNS, the number of fibroblasts are increased after spinal cord injury, and these fibroblasts secrete extracellular matrix molecules to protect the lesion site (Kawano et al., 2012; O'Shea et al., 2017; Dorrier et al., 2021). In the PNS, fibroblasts in the DRG meninges participate in the regulation of neuropathic pain. After spared nerve injury, fibroblasts expand to increase the thickness of the DRG meninges and secrete the protease inhibitor PI16 after nerve injury. Fibroblast-derived PI16 is a crucial signal for establishment of chronic neuropathic pain through promoting immune cell infiltration (Singhmar et al., 2020). In short, fibroblasts secrete excessive extracellular matrix proteins to play different roles according to their organ of origin and spatial distribution (Nash et al., 2004; Kawano et al., 2012).

Secreted modular calcium-binding protein 2 (SMOC2) is an extracellular calcium-binding protein that belongs to the secreted protein acidic and rich in cysteine (SPARC) family of modular extracellular proteins. SMOC2 was first isolated from a screen of a mouse brain cDNA library (Vannahme et al., 2003). It is expressed in different tissues of adult mice, such as ovary, heart, muscle, and spleen (Vannahme et al., 2003). SMOC2 activates fibroblast-to-myofibroblast transition to stimulate the stress fiber formation during kidney fibrosis (Gerarduzzi et al., 2017), and upregulation of SMOC2 accelerates the bleomycin-induced development of pulmonary fibrosis (Luo et al., 2018). SMOC2 participates in the regulation of cell cycle and DNA synthesis via integrin-linked kinase (Liu et al., 2008). In addition, SMOC2 contributes to the progression of colon cancer (Shvab et al., 2016) and modulates the activity of angiogenic growth factor (Rocnik et al., 2006). However, the expression and function of SMOC2 in the nervous system are still unknown.

In the present study, we show that SMOC2 is mainly expressed in fibroblasts in the DRG. The fibroblast-secreted SMOC2 in the DRG is specifically required for maintaining the mechanical threshold. SMOC2 suppresses coupled activation of adjacent DRG neurons induced by noxious mechanical stimuli through inhibiting the function of satellite glial P2X7 receptor (P2X7R). This study reveals a critical role of fibroblast-secreted protein in maintaining nociceptive sensation.

Materials and Methods

Animals. Experiments involving mice were performed according to the guidelines of the Committee for Research and Ethical Issues of the International Association for the Study of Pain, and were approved by the Animal Care and Use Committee of the Institute of Neuroscience, Chinese Academy of Sciences, Shanghai, China. C57BL/6J mice were purchased from Shanghai Laboratory Animal Center, Chinese Academy of Sciences (Shanghai, China). *Smoc-2*$^{-/-}$ mice were initially acquired from the Mutant Mouse Resource and Research Center (049781-UCD). Mice (2–4 months old) were raised under a 12 h light/dark cycle at 22°C–26°C (lights on at 7:00 A.M.) with food and water supply. Mice were assigned randomly into different groups.

Plasmid construction. Mouse SMOC2 cDNA was subcloned into pcDNA3.1A(−)-Myc-His with the following 5′ and 3′ primers: 5′-ATGCTGCCGCCACAGCTGTGCTGGC-3′ and 5′-TCCTTGTTTCCTGGGCTGTCTATTA-3′. Mouse connexin 43 (CX43) cDNA was subcloned into pECMV-Flag and pcDNA3.1-mCherry with the following 5′ and 3′ primers: 5′-ATGGGTGACTGGAGCGCCTTGGGGA-3′ and 5′-AATCTCCAGGTCATCAGGCCGAGGT-3′. Mouse P2X7R cDNA was subcloned into pECMV-Flag with the following 5′ and 3′ primers: 5′-ATGCCGGCTTGCTGCAGCTG-3′ and 5′-GTAGGGATACTTGAAGCCACTATAC-3′.

Behavioral tests. Behavioral tests were performed with 2-month-old male mice. All mice were placed in the experimental environment at least 1 h per day for over 3 d before behavioral tests. Behavioral tests were conducted blindly. In the von Frey test, the thresholds of nociceptive mechanical stimuli of both male and female mice were measured. In Hargreaves tests, the responses of both male and female mice to the radiant heat were recorded. In the other behavioral tests, we used male mice only. In the tail flick and hot plate tests, the response latency to noxious thermal stimuli was recorded. The tests above were stopped at a cutoff time or force for animal protection. In the formalin test, the duration of nociceptive responses was recorded. In the itch test, the times of scratch were recorded. All the behavioral tests were performed in a blinded way.

von Frey test. The mouse was habituated in a plastic chamber on mesh floor for over 30 min before the formal test. The mechanical threshold was measured by the von Frey filaments (Ugo Basile) with forces of increasing grades applied to the left hindpaw of mouse. One filament was applied at most 5 times with 10 s interval in a round of testing and then switched to the next filament of either bigger force (if negative response occurred three times) or smaller force (if positive response occurred 3 times).

Hargreaves test. The mouse was habituated in a plastic chamber on glass floor, and radiant light (Ugo Basile) was applied to its left hindpaw. The mouse was stimulated with the radiant light when it was resting quietly, and the light was stopped immediately after the hindpaw movement. The cutoff time of radiant light was 20 s.

Tail flick test. The tail of mouse was immersed in a water bath at 52°C. The cutoff time was 10 s.

Hot plate test. Mouse was put on a hot plate (Ugo Basile) at a temperature of 52°C, and the cutoff time was 30 s.

Rotarod test. The mouse was tested on a rotarod with the velocity increasing from 4 to 40 rpm within 5 min. The mouse was trained for 2 d before the formal test. The duration time on the rotarod before the mouse fell off was recorded.

Open field test. The mouse was put in an open field apparatus (45 × 45 cm), and its exploratory locomotor activity within 30 min was recorded. The total moving distance and the moving velocity were measured during the whole procedure.

Formalin test. The 0.5% formalin (Sigma) diluted in saline was intradermally injected into the left hindpaw of the mouse. The spontaneous nociceptive responses were recorded for 40 min, and the duration of licking or biting behavior was counted with a 5 min interval. The first phase of nociceptive response was during 0–10 min, and the second phase of nociceptive response was during 10–40 min.

Itch test. The mouse was put in a plastic chamber on mesh floor for 30 min adaption. The mouse was intradermally injected pruritic compound at the right back neck at a volume of 50 μl. The time of hindlimb scratching behavior toward the injection site was measured for 30 min

with 5 min intervals. The pruritogen was dissolved in sterile saline for histamine (500 μg/50 μl), 5-hydroxytryptamine (10 μg/50 μl), and chloroquine (200 μg/50 μl) (Sigma).

RNAscope assay. The probes and detection kit of RNAscope were purchased from Advanced Cell Diagnostics. The RNAscope 2.5 HD Detection Reagent-RED (catalog #322360) was used for the bright-field detection. The sections from L4 and L5 DRGs were hybridized with *Smoc2* probes (catalog #318541) according to the manufacturer's instruction. The images were collected with Zeiss microscope (Axio Imager M2).

In vivo *siRNA injection.* Before the injection, each mouse was habited in the behavior room for 3 d. The basal mechanical threshold and heat latency were tested. Then, 0.8 μg si*Smoc2* or scramble siRNA was injected to the bilateral L4 and L5 DRGs of these mice randomly. After 3 d, von Frey and Hargreaves tests were performed. Then the L4 and L5 DRGs were harvested for RNA extraction. RT-PCR was performed to check the efficiency of *Smoc2* knockdown. The siRNA sequences were as follows: sense 5′-UUCUCCGAACGUGUCACGUTT-3′ and antisense 5′-ACGUGACACGUUCGGAGAATT-3′ for scramble siRNA, and sense 5′-GCGACAUGAACAAUGACAATT-3′ and antisense 5′-UUGUCAUUGUUCAUGUCGCTT-3′ for si*Smoc2*. All the behavioral tests and siRNA injection were performed in a blind way.

RNA extraction and qPCR. Total RNA was isolated using Trizol reagent (Invitrogen), and mRNA was reverse-transcribed into cDNA with SuperScript II reverse transcriptase (Invitrogen). qPCR was performed with Premix Ex Taq (Takara). The expression of *Smoc2* was detected using following primers: 5′-ACAGCTAGACTACATCGTCCCA-3′ and 5′-TCCAGTTCATAACCTTCATCCC-3′.

Cell culture and transfection. HEK293 cells (National Collection of Authenticated Cell Cultures) were cultured in MEM (Invitrogen) with 10% FBS (Ausbian). COS7 cells (National Collection of Authenticated Cell Cultures) were cultured in DMEM (Invitrogen) with 10% FBS. The cells were transfected 4-6 μg plasmid per 60 mm dish using PEI reagent (Millipore Sigma). The cells were used for the following experiments 24-48 h after transfection.

The DRGs were isolated from the C57BL/6J mice and digested as previously described (Yang et al., 2017). The dissociated cells were naturally subsided for 15 min in a small dish at cell incubator to acquire the non-neuronal DRG cells. The fibroblasts were incubated in DMEM with 10% FBS for proliferation and then used for the experiment of SMOC2 secretion or transferred to the 12-well plate for siRNA transfection.

Coimmunoprecipitation and immunoblotting. The DRGs or cultured cells were homogenized in RIPA buffer (30 mM HEPES, pH 7.5, 10 mM NaF, 150 mM NaCl, 0.01% SDS, and 1% Triton X-100) or cell lysis buffer (50 mM Tris-HCl, pH 7.5, 150 mM NaCl, 0.1% Triton X-100, 10% glycerol, and 0.05% BSA) with protease inhibitors (1 mM PMSF, 10 mg/ml aprotinin, 1 mg/ml pepstatin, and 1 mg/ml leupeptin; Roche). The cell supernatants were incubated with Flag antibody (Sigma, F7425), and the tissue supernatants were incubated with IgG or P2X7R antibody (Alomone Labs, APR-004) overnight at 4°C. Afterward, protein G beads (Roche) were incubated at 4°C for 2 h. The immunoprecipitates and total lysates were applied for immunoblotting. The samples were boiled at 100°C for 5 min denature, loaded for SDS-PAGE, transferred, probed with antibodies, and visualized with enhanced chemiluminescence. Primary antibody was applied overnight at 4°C, and secondary antibody was applied for 1 h at room temperature. The bands of specific protein were visualized with chemiluminescence. The primary antibodies include that against SMOC2 (1:500; Santa Cruz Biotechnology, sc-55 295), P2X7 (1:1000; Alomone Labs, APR-004), actin (1:4,000,000; Chemicon, MAB1501), Flag (1:2000; Sigma, F3165), and Myc (1:1000; Proteintech, 60003-2-lg).

Cell-surface biotinylation. The cells were treated by DMEM with 1% FBS for 1 and 4 h. Then, the cells were cooled on ice immediately and washed by Ca^{2+}/Mg^{2+} PBS. Sulfo-NHS-LC-Biotin (Pierce Protein Biology) was added into each cell culture medium at a working concentration of 0.25 mg/ml for 45 min at 4°C. The cells were lysed with 400 μl cell lysis buffer, 30 μl lysate was used as a whole-cell sample, and the remainder was precipitated with streptavidin-agarose beads (Pierce Protein Biology) overnight at 4°C. The precipitated sample was denatured and prepared for immunoblotting.

In vivo *calcium imaging.* To express GCaMP6s specifically in DRG neurons, AAV2/9-CAG-GCaMP6s (Taltool) was injected into left L4/5 DRGs of adult C57/BL6 mice or *Smoc2*$^{-/-}$ mice. Mice were anesthetized during the whole experiment with 1.5% isoflurane gas using a gas anesthesia apparatus (RWD, China). *In vivo* calcium imaging and data analysis were performed in a blinded way.

The L4/5 DRGs were exposed again 1 month after injection of GCaMP6s-carrying virus. The spinal column was immobilized using a custom-designed adapter for spinal cord (RWD) to minimize the effects caused by breath and heartbeat. Nociceptive mechanical pinch stimuli were applied to the left hindpaw of mice by the toothed forceps, and strong pressure stimuli was applied by flat tweezers. Noxious heat stimuli were applied to the hindpaw of mice by 55°C hot water. The intensity of calcium fluorescence was recorded in real time by an Olympus two-photon microscope with a 2 mm working distance, 25× water immersion lens (numerical aperture, 1.05). A mode-locked InSight X3-OL femtosecond IR laser (Spectra-Physics) generated two-photon excitation at 960 nm, and two thermoelectric/air-cooled GaAsP photomultiplier tubes (Hamamatsu) collected the emitted light in ranges of 495-540 and 575–645 nm. The power reaching the mouse DRG ranged from 7 to 15 mW. Images were acquired at 66 ms/frame at a resolution of 512 × 512 pixels for 4000 frames. The process of stimuli included 1 min for rest, 2.5 min for stimuli, and 1 min for rest. The interval between any two thermal or nociceptive mechanical stimuli was 3-5 min to avoid sensitization. The SMOC2 protein or A740003 was injected to the recorded DRG, and then the second record was performed at the same place of DRG after 30 min. The influence of breath was filtered.

HEK293 cells were transfected with plasmid of P2X7R for 24 h. Then, cells were loaded for at least 30 min in the dark with 2 μM Fluo-4AM (Invitrogen) followed by incubating with 50 nM SMOC2 protein (R&D Systems), 100 μM A740003 (Tocris Bioscience), or vehicle at 37°C in the extracellular solution (140 mM NaCl, 3 mM KCl, 2 mM $MgCl_2$, 2 mM $CaCl_2$, 10 mM HEPES, 10 mM D-glucose, pH 7.3) for 30 min. Afterward, the calcium activity of cells responding to 1 mM ATP (Sigma) was monitored. The data were analyzed as previously described (Kim et al., 2016).

Immunohistochemistry. The mouse was anesthetized and perfused via the ascending aorta with warm saline (37°C) followed by warm solution composed of 4% PFA. The perfusion was then followed by the same fixative (4°C) for another 3 min, and L4/L5 DRGs were dissected and sectioned. After blocked with PBS containing 0.05% Triton X-100 and 10% donkey serum, slices were incubated with isolectin B4 (IB4, 1:1000, FL-1201, Vector Laboratories), or primary antibodies against calcitonin gene-related peptide (CGRP) (1:1000; Dia Sorin, 24112), neurofilament 200 (NF200, 1:10,000; Abcam, ab4680), NEUN (1:2000; Millipore, ABN90), fatty acid binding protein 7 (FABP7, 1:5000; Abcam, ab32423), platelet-derived growth factor receptor α (PDGFRα, 1:1000; CST, 3174), and Collagen IV (1:2000; Merck, AB756P) overnight at 4°C, and followed with secondary antibodies (Invitrogen) for 40 min at room temperature. The slices were mounted and imaged by Leica SP8 confocal microscope and Leica TCS SP8 STED X.

More than 3 mice were used for every single immunostaining experiment, and bilateral L4 and L5 DRGs of all mice were collected for each group. The images of whole DRGs were taken by confocal Leica SP8. To do the quantitative analysis of cell number in single DRG, the total DRG neurons marked by neuronal nuclei (NeuN), fibroblasts marked by PDGFRα, and SGCs marked by FAPB7 on the three nonadjacent sections were counted. The average number of at least three DRGs with three nonadjacent slices represents one sample. When analyzing the diameter of DRG neurons, only neurons with DAPI staining were counted.

Experimental design and statistical analysis. Data are presented as mean ± SEM. Sample number (n) is indicated in the figure legends. Two groups were compared by a two-tailed, paired or unpaired Student's t test. Comparison between two groups with multiple times was performed by a two-way ANOVA followed by Bonferroni's *post hoc* test. Multiple groups were compared by a one-way ANOVA followed by

Tukey's *post hoc* test. Statistical analysis was performed using PRISM (GraphPad Software). We also tested whether the data conform to the normal distribution with the normality and log-normality tests in GraphPad Prism before one-way or two-way ANOVA. The significant difference was considered at $p < 0.05$. Three nonadjacent slices were used for statistical analysis. All the image analyses were performed in a blinded way.

Results

SMOC2 is expressed in DRG fibroblasts

To explore the expression of SMOC2 in the DRG, we reanalyzed the transcriptome of single cells dissociated from lumber (L)4 and L5 DRG by 10× Genomics (Wang et al., 2021). The single-cell RNA sequencing data of DRGs revealed that *Smoc2* was expressed neither in DRG neurons marked by NeuN, encoded by *Rbfox3* nor in SGCs marked by FABP7, encoded by *Fabp7*. Surprisingly, *Smoc2* in the DRG was expressed in fibroblasts labeled by an intracellular marker, PDGFRα, encoded by *Pdgfra* (Fig. 1*A*). Both immunostaining with specific SMOC2 antibody and RNAscope showed that SMOC2 was distributed in non-neuronal cells surrounding DRG neurons (Fig. 1*B–D*). Additionally, SMOC2 was not present in DRG neurons labeled by CGRP, IB4, or NF200 (Fig. 1*E*). Indeed, SMOC2 was colocalized with PDGFRα, a marker of fibroblasts (Fig. 1*F*,*G*), consistent with the single-cell RNA sequencing result. The SMOC2-positive ($^+$)/PDGFRα$^+$ fibroblasts in DRGs displayed a spindle shape and had pseudopodia at both ends to surround DRG neurons (Fig. 1*G*). To further identify the relationship among DRG neurons, SGCs, and fibroblasts, we costained their markers, including NeuN, FABP7, and SMOC2. Immunostaining showed that DRG neurons were surrounded by FABP7$^+$ SGCs as previously reported (Hanani, 2005). Importantly, SMOC2$^+$ fibroblasts encircled a DRG neuron and its attached SGCs (Fig. 1*H*,*I*), suggesting that fibroblasts could further obstruct the connection of adjacent DRG neurons mediated by SGCs.

As a member of SPARC family, SMOC2 is considered as a secretory protein. The secreted potentiality of SMOC2 was further examined in primary cultured fibroblasts derived from adult mouse DRGs. The protein secreted to the culture medium by the cultured DRG fibroblasts was precipitated by trichloroacetic acid after 1 or 4 h of serum starvation. Immunoblotting with the antibody against SMOC2 showed that the level of SMOC2 in the culture medium was increased as time went on (Fig. 1*J*), suggesting a spontaneous secretion of SMOC2 from fibroblasts. To examine whether the secreted SMOC2 was adhered to the cell membrane, the cell-surface protein of cultured DRG fibroblasts was precipitated by the experiment with surface biotinylation, and the existence of SMOC2 was detected by immunoblotting. The result showed that SMOC2 tended to adhere to the plasma membrane over time (Fig. 1*K*), implying that SMOC2 could be secreted by the DRG fibroblasts to serve as an extracellular matrix. Interestingly, immunostaining showed that SMOC2 was colocalized with Collagen IV, a marker of basement membrane (Fig. 1*L*), suggesting that SMOC2 secreted from fibroblasts is a component of the basement membrane in DRGs. The basement membrane is thin connective tissue structure and is composed of ubiquitous extracellular protein matrices (Saikia et al., 2018). The constituent protein of basement membrane influences cells by interacting with receptors on the plasma membrane (Ohara et al., 2009; Yurchenco, 2011; Pozzi et al., 2017). The basement membrane is also regarded as a barrier for cell penetration and provides tissue compartmentalization (Timpl, 1996). Together, SMOC2 is expressed in fibroblasts and secreted to be a component of the basement membrane.

SMOC2 is required for mechanical nociception

After determining the distribution of SMOC2 in the DRG, we explored the physiological functions of fibroblastic SMOC2 in nociceptive sensation. We obtained *Smoc2* KO (*Smoc2*$^{-/-}$) mice and first evaluated the KO efficiency of *Smoc2*. The qPCR showed that *Smoc2* was almost undetectable in *Smoc2*$^{-/-}$ mice compared with *Smoc2*$^{+/+}$ mice (1.000 ± 0.313 for *Smoc2*$^{+/+}$ mice and 0.018 ± 0.006 for *Smoc2*$^{-/-}$ mice, $t = 2.689$, $df = 12$, $p = 0.020$) (Fig. 2*A*). Next, we detected the behavioral responses of *Smoc2*$^{-/-}$ mice, including nociceptive responses, motor activities, and itch sensations. Surprisingly, in the von Frey test, the nociceptive mechanical threshold was remarkably reduced in male and female *Smoc2*$^{-/-}$ mice ($F_{(1,17)} = 2.429$, $p = 0.138$; male: 1.044 ± 0.080 for *Smoc2*$^{+/+}$ mice and 0.556 ± 0.029 for *Smoc2*$^{-/-}$ mice, $t = 5.941$, $df = 17$, $p < 0.001$; female: 0.880 ± 0.085 for *Smoc2*$^{+/+}$ mice and 0.452 ± 0.077 for *Smoc2*$^{-/-}$ mice, $t = 5.482$, $df = 17$, $p < 0.001$) (Fig. 2*B*). These results indicate that SMOC2 has a marked effect on nociceptive mechanical response under physiological condition in mice of both sexes. However, the Hargreaves results showed that the loss of SMOC2 did not affect the response latency of *Smoc2*$^{-/-}$ mice to radiant heat stimulus compared with *Smoc2*$^{+/+}$ mice in both sexes ($F_{(1,15)} = 3.778$, $p = 0.071$) (Fig. 2*C*). We also tested the effect of SMOC2 to heat nociception with other noxious heat stimuli. Both hot plate and tail immersion results confirmed that loss of SMOC2 did not affect the response of mice to the noxious heat stimuli (Fig. 2*D*,*E*). The accelerated rotarod test and open field test showed that *Smoc2*$^{-/-}$ mice did not exhibit obvious defects in the motor ability (Fig. 2*F–H*). Moreover, we investigated the effect of SMOC2 in an acute chemical pain model induced by intraplantar injection of 0.5% formalin, which causes a stereotypic two-phase phenomenon of nociceptive response. The *Smoc2*$^{-/-}$ mice showed similar licking times in Phase I and II of formalin test compared with *Smoc2*$^{+/+}$ mice (Fig. 2*I*,*J*). In addition, we also tested whether loss of SMOC2 affected the itch sensation of mice. Scratching behavior was assessed by intradermally injecting histamine, 5-hydroxytryptamine, or chloroquine into the right side of mouse nape, and the number of bouts in right hindpaw scratching directed toward the injection site was analyzed. The results showed that the number of bouts induced by pruritogens in *Smoc2*$^{-/-}$ mice was similar to that in *Smoc2*$^{+/+}$ mice (Fig. 2*K–M*). Therefore, *Smoc2* KO mice exhibit a selective defect in nociceptive mechanical response.

Since SMOC2 was also detected to be expressed in several other tissues (Vannahme et al., 2003), we further explored whether the decrease of nociceptive mechanical threshold in *Smoc2*$^{-/-}$ mice was caused by a specific loss of SMOC2 in the DRG. *In vivo* knockdown of *Smoc2* in the DRG was adopted by directly injecting *Smoc2* siRNA into the L4 and L5 DRGs. qPCR showed that the expression of *Smoc2* was decreased to $41.4 \pm 6.0\%$ in primary cultured DRG fibroblasts after application of *Smoc2* siRNA compared with scramble siRNA ($t = 9.830$, $df = 2$, $p = 0.010$) (Fig. 3*A*). We then injected *Smoc2* siRNA or scramble siRNA into the ipsilateral or contralateral L4 and L5 DRGs of the same mouse, respectively (Fig. 3*B*). After 3 d of injection, we measured the nociceptive mechanical threshold and response latency to noxious thermal stimuli. As expected, the von Frey test showed that, after knockdown of *Smoc2* in ipsilateral L4 and L5 DRGs, the mechanical thresholds of hindpaws of both male and female mice were significantly decreased compared with the contralateral hindpaws innervated by L4 and L5

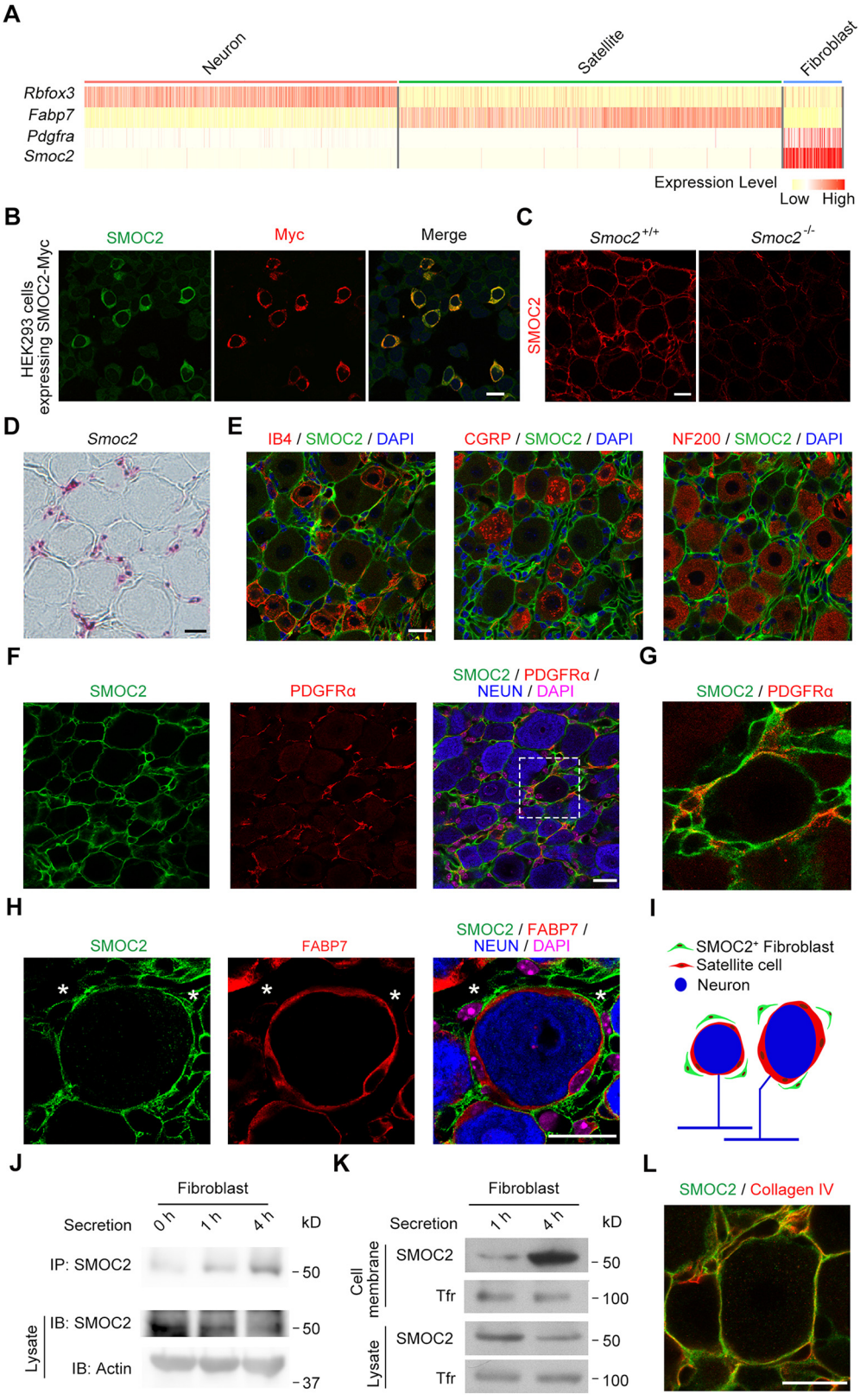

Figure 1. SMOC2 is expressed in fibroblasts in the DRG. ***A***, Single-cell RNA sequencing showing the expression profile of *Rbfox3*, *Fabp7*, *Pdgfra*, and *Smoc2* in the DRG. ***B***, ***C***, Immunostaining showing the specificity of SMOC2 antibody in HEK293 cells expressing SMOC2-Myc (***B***) and the DRG of $Smoc2^{-/-}$ mice (***C***). ***D***, RNAscope showing *Smoc2*-positive puncta expressed around DRG neurons. ***E***, Immunostaining showing that SMOC2 (green) was not coexpressed with IB4, CGRP, or NF200 (red) in DRG neurons. ***F***, ***G***, Immunostaining showing that SMOC2 (green) was colocalized with PDGFRα (red) in DRG fibroblasts. The image within white dotted line was magnified (***G***). ***H***, Immunostaining showing that the expression of SMOC2 (green) was around DRG neurons and its attached SGCs. ***I***, Diagram represents the distribution of fibroblast, SGC, and neuron in the DRG. ***J***, Immunoblotting showing that the SMOC2 level was increased with incubation time in the culture medium of mouse DRG fibroblasts. ***K***, Immunoblotting showing that the secreted SMOC2 tended to adhere to the cell membrane. ***L***, Immunostaining showing that SMOC2 (green) was colocalized with Collagen IV (red) in the DRG. Scale bar, 20 μm.

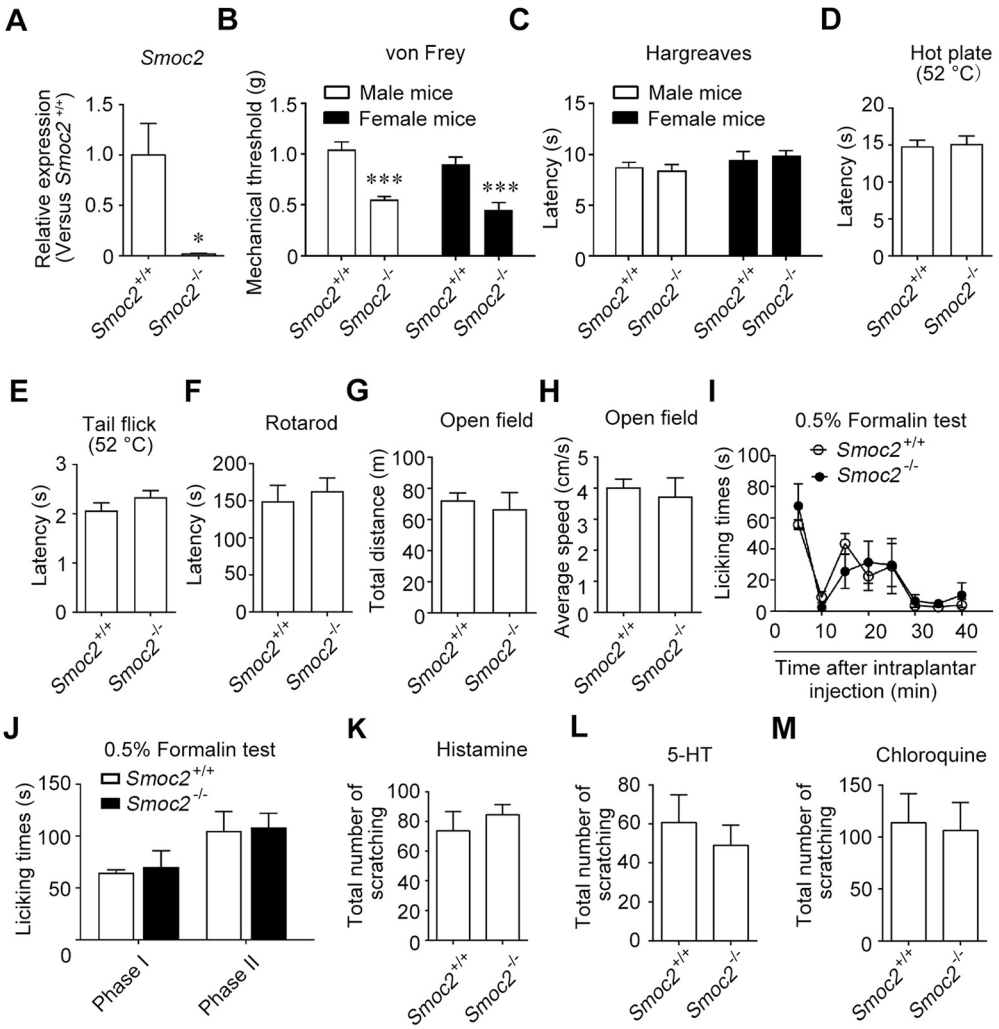

Figure 2. KO of *Smoc2* leads to the decreased nociceptive mechanical threshold of mice. ***A***, qPCR showing that *Smoc2* was not detected in the DRG of $Smoc2^{-/-}$ mice ($n = 8$). ***B***, The mechanical threshold of $Smoc2^{-/-}$ mice was decreased compared with that of $Smoc2^{+/+}$ mice in von Frey test in both sexes (male: $n = 9$; female: $n = 10$). ***C***, The noxious thermal latency of $Smoc2^{-/-}$ mice was not altered compared with that of $Smoc2^{+/+}$ mice in Hargreaves test in both sexes (male: $n = 9$; female: $n = 8$). ***D***, ***E***, The latency to noxious thermal stimuli was unchanged between $Smoc2^{+/+}$ and $Smoc2^{-/-}$ mice ($n = 8$) in both hot plate and tail flick tests. ***F***, The drop latency of $Smoc2^{-/-}$ mice was unchanged compared with that of $Smoc2^{+/+}$ mice ($n = 9$) in rotarod test. ***G***, ***H***, $Smoc2^{-/-}$ mice had no defects in the motor ability in open field test ($n = 4$ for $Smoc2^{+/+}$ mice; and $n = 3$ for $Smoc2^{-/-}$ mice). ***I***, ***J***, $Smoc2^{-/-}$ mice did not show any apparent changes in the flinch number of either the first phase or the second phase in formalin test ($n = 4$ for $Smoc2^{+/+}$ mice; and $n = 3$ for $Smoc2^{-/-}$ mice). ***K-M***, The scratching number induced by histamine, 5-hydroxytryptamine, and chloroquine in $Smoc2^{-/-}$ mice ($n = 6$) was similar to that in $Smoc2^{+/+}$ mice ($n = 7$). Data are mean ± SEM. $^{*}p < 0.05$, $^{***}p < 0.001$ versus $Smoc2^{+/+}$ mice: (***A***,***D-H***,***K-M***) two-tailed unpaired *t* test; (***B***,***C***,***I***,***J***) two-way ANOVA with Bonferroni correction.

DRGs injected with scramble siRNA (male: $F_{(1,24)} = 5.124$, $p = 0.032$; si*Smoc2*: 0.908 ± 0.066 to 0.462 ± 0.027, $t = 6.624$, df = 24, $p < 0.001$; female: $F_{(1,8)} = 20.630$, $p = 0.002$; si*Smoc2*: 1.080 ± 0.080 to 0.480 ± 0.049, $t = 5.071$, df = 8, $p = 0.002$) (Fig. 3*C*,*D*). Immediately after behavioral tests, bilateral L4 and L5 DRGs were separately collected and reverse transcription was then performed to examine the knockdown efficiency of *Smoc2* in DRGs. qPCR showed that *Smoc2* in the ipsilateral DRGs was decreased to 42.7 ± 5.8% in male mice and to 38.9 ± 7.7% in female mice of von Frey test ($F_{(1,16)} = 0.1304$, $p = 0.723$; male: $t = 10.260$, df = 16, $p < 0.001$; female: $t = 6.788$, df = 16, $p < 0.001$) (Fig. 3*E*). Meanwhile, the response latency to noxious heat stimuli was not changed after the si*Smoc2* injection in mouse DRGs of both sexes, suggesting that knockdown of *Smoc2* in the DRG did not affect the noxious thermal sensation (Fig. 3*F–H*). The effect of *in vivo Smoc2* knockdown in the DRG was similar to that of genetic KO, indicating that the increased mechanical sensitivity of $Smoc2^{-/-}$ mice is because of loss of SMOC2 in the DRG. Together, fibroblast-secreted SMOC2 in the DRG specifically contributes to the nociceptive mechanical sensation.

Loss of SMOC2 leads to an increase of clustered neurons in the DRG

Since $Smoc2^{-/-}$ mice showed mechanical hypersensitivity under normal condition, we examined the morphologic change of DRGs induced by loss of SMOC2. Immunostaining showed that the number of PDGFRα^{+} fibroblasts was not changed in the DRG of $Smoc2^{-/-}$ mice compared with that of control mice (Fig. 4*A*,*B*). Using dual-fluorescence immunostaining, the colocalization of SMOC2 with Collagen IV was detected in the DRG. Although most neurons were surrounded by Collagen IV^{+} basement membrane in $Smoc2^{+/+}$ mice, ~24.4 ± 2.2% neurons were clustered together with several adjacent neurons whose Collagen IV^{+} basement membrane were lost (Fig. 4*C*,*D*). The clustered neurons were first defined as two or more of DRG neurons surrounded by a common connective envelope (Pannese et al.,

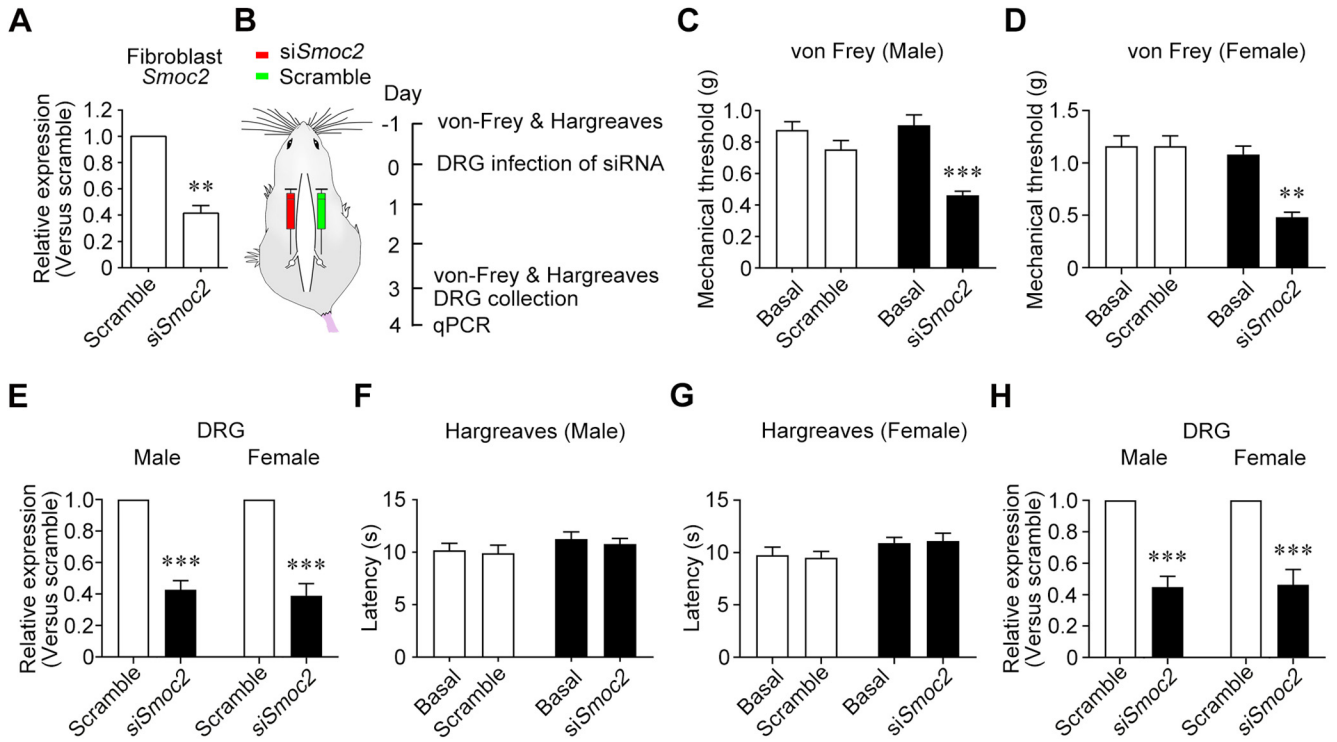

Figure 3. SMOC2 in the DRG is required for maintaining nociceptive mechanical threshold. ***A***, qPCR showing that the expression of *Smoc2* was reduced in the cultured DRG fibroblasts after si*Smoc2* treatment ($n = 3$). ***B***, Flowchart represents the process of behavioral tests and si*Smoc2* injection in mice. The L4 and L5 DRGs were injected with si*Smoc2*. The von Frey and Hargreaves tests were performed before and 3 d after si*Smoc2* injection, respectively. The knockdown efficiency of si*Smoc2* in the L4 and L5 DRGs of mice was detected after behavioral tests. ***C***, The nociceptive mechanical threshold of male mice was reduced after the knockdown of *Smoc2* in L4 and L5 DRGs ($n = 13$). ***D***, The nociceptive mechanical threshold of female mice was reduced after the knockdown of *Smoc2* in L4 and L5 DRGs ($n = 5$). ***E***, qPCR showing that the expression of *Smoc2* was reduced in L4 and L5 DRGs of both sexes of mice after si*Smoc2* injection and von Frey test. ***F***, The noxious thermal latency of male mice was not changed after knockdown of *Smoc2* in L4 and L5 DRGs ($n = 9$). ***G***, The noxious thermal latency of female mice was not changed after knockdown of *Smoc2* in L4 and L5 DRGs ($n = 6$). ***H***, qPCR showing that the expression of *Smoc2* was reduced in L4 and L5 DRGs of both sexes of mice after si*Smoc2* injection and Hargreaves. Data are mean ± SEM. $^{**}p < 0.01$, $^{***}p < 0.001$ versus scramble siRNA: (***A***) two-tailed paired *t* test; (***C-H***) two-way ANOVA with Bonferroni correction.

1991, 1993). Since the basement membrane is a structure with thin connective tissue, here we used the notion of clustered neurons to refer two or more of DRG neurons surrounded by the basement membrane containing SMOC2 and Collagen IV. Notably, the percentage of clustered DRG neurons was increased to 43.9 ± 0.9% in $Smoc2^{-/-}$ mice ($t = 17.970$, df = 4, $p < 0.001$) (Fig. 4*C*,*D*), suggesting that SMOC2 is required for the formation of basement membrane impeding clustered neurons in the DRG. We also quantified the diameter of these clustered neurons. The statistic results showed that most clustered neurons were small neurons to small or medium neurons in the DRG of both $Smoc2^{-/-}$ mice and control mice (Fig. 4*E*). Meanwhile, the distribution of SGCs was checked in clustered DRG neurons of $Smoc2^{-/-}$ mice. Immunostaining showed that both clustered DRG neurons and nonclustered DRG neurons were tightly surrounded by $FABP7^{+}$ SGCs (Fig. 4*F*). These results suggest that loss of SMOC2 increases the number of clustered neurons in the DRG.

Loss of SMOC2 increases coupled activation of adjacent neurons in the DRG

In the DRG, adjacent neurons tend to be activated together through increased cell communication after peripheral inflammation or nerve injury (Dublin and Hanani, 2007; Song et al., 2014). Inhibiting the coupled activation of adjacent DRG neurons attenuates the mechanical hypersensitivity induced by inflammation (Kim et al., 2016). Since SMOC2 deficiency increased the percentage of clustered neurons in the DRG, we considered the possibility that fibroblast-secreted SMOC2 could obstruct the coupled activation of adjacent neurons to maintain normal nociceptive mechanical threshold. To this end, the neuronal activity was monitored by *in vivo* DRG calcium imaging with the application of nociceptive mechanical or noxious heat stimulation to the left hindpaw of anesthetic male and female mice (Fig. 5*A*). Neuronal coupling was defined as in a previous report, in which two or more adjacent DRG neurons were synchronously activated by the same stimulus (Kim et al., 2016). We injected recombination adeno-associated virus-expressing GCaMP6s, a genetically encoded fluorescent calcium indicator, into the left L4 and L5 DRGs of mice. First, we studied the effect of SMOC2 on the activation of DRG neurons induced by nociceptive mechanical stimulus. The calcium imaging of DRG neurons showed that the majority of DRG neurons in response to pinch were activated individually in $Smoc2^{+/+}$ mice (Fig. 5*B*), which was consistent with a previous report (Kim et al., 2016). Only 18.8 ± 1.2% of responsive neurons displayed a coupled activation in male $Smoc2^{+/+}$ mice (Fig. 5*C*). Notably, 42.3 ± 2.5% of activated neurons were coupled in male $Smoc2^{-/-}$ mice, which was remarkably higher than that in $Smoc2^{+/+}$ mice ($t = 5.709$, df = 22, $p < 0.001$) (Fig. 5*C*). In total, 29.6 ± 2.5% of virus-infected neurons were coupled activated in male $Smoc2^{-/-}$ mice, while only 10.4 ± 0.6% of these neurons displayed similar phenomena in male $Smoc2^{+/+}$ mice ($t = 5.941$, df = 22, $p < 0.001$) (Fig. 5*D*). Moreover, the number of total activated neurons was also increased in male $Smoc2^{-/-}$ mice compared with male

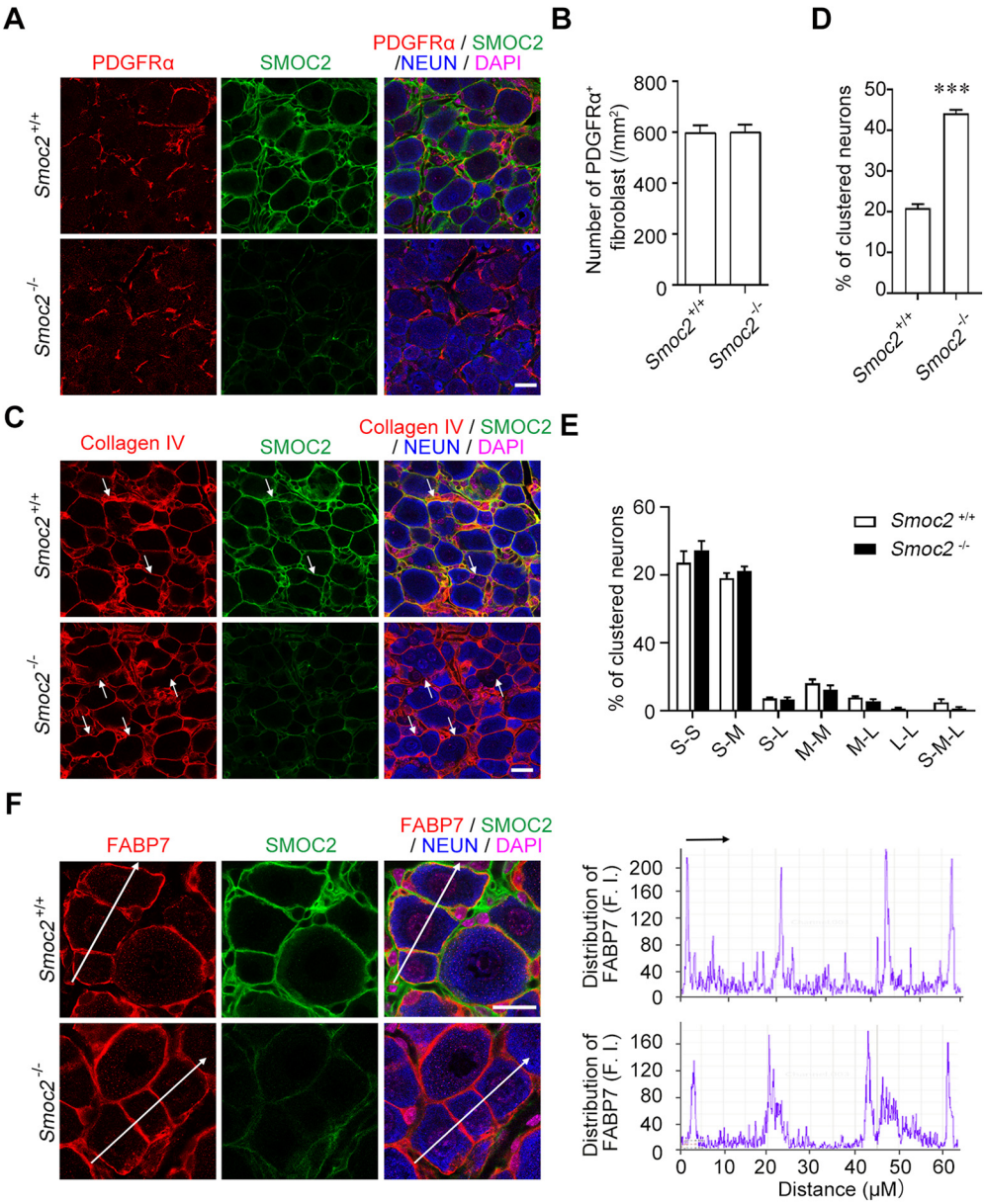

Figure 4. Loss of SMOC2 increases clustered neurons in the DRG. ***A***, Immunostaining showing the expression of PDGFRα^+ fibroblasts in the DRG of *Smoc2*$^{+/+}$ and *Smoc2*$^{-/-}$ mice. ***B***, The quantitative data showed that the number of PDGFRα^+ fibroblasts per square millimeter of DRG soma was not changed in *Smoc2*$^{+/+}$ and *Smoc2*$^{-/-}$ mice ($n = 3$). ***C***, Immunostaining showing the expression of Collagen IV (red) in the DRG of *Smoc2*$^{+/+}$ and *Smoc2*$^{-/-}$ mice. White arrow indicates the clustered DRG neurons. ***D***, The quantitative data showed that the percentage of clustered DRG neurons surrounded by Collagen IV was increased in the DRG of *Smoc2*$^{-/-}$ mice compared with that of *Smoc2*$^{+/+}$ mice. ***E***, Percentage of clustered neuron was not changed according to the size of each member of the pair in the DRG of both *Smoc2*$^{+/+}$ mice and *Smoc2*$^{-/-}$ mice. S, Small-diameter DRG neurons (<20 μm); M, medium (20-30 μm); L, large (>30 μm). ***C-E***, $n = 5$ for *Smoc2*$^{+/+}$ mice and $n = 6$ for *Smoc2*$^{-/-}$ mice. ***F***, The expression of FABP7$^+$ SGCs was not changed in the DRG of *Smoc2*$^{-/-}$ mice compared with that of *Smoc2*$^{+/+}$ mice. Right, Chart represents the fluorescent intensity (F.I.) of FABP7 around the DRG neuron. Scale bar, 20 μm. Data are mean ± SEM. ***$p < 0.001$ versus *Smoc2*$^{+/+}$ mice: (***B***,***D***) two-tailed unpaired *t* test; (***E***) two-way ANOVA with Bonferroni correction.

Smoc2$^{+/+}$ mice (55.6 ± 1.3% for *Smoc2*$^{+/+}$ mice and 69.8 ± 3.2% for *Smoc2*$^{-/-}$ mice, $t = 3.840$, df = 22, $p = 0.002$) (Fig. 5*E*), implying that some neurons hijacked their adjacent neurons to simultaneously respond to pinch because of loss of SMOC2 in the DRG. The coupled activation of DRG neurons in female *Smoc2*$^{-/-}$ and *Smoc2*$^{+/+}$ mice was similar to that of male mice (Fig. 5*C*, $F_{(1,22)} = 0.075$, $p = 0.787$; Fig. 5*D*, $F_{(1,22)} = 0.185$, $p = 0.671$; Fig. 5*E*, $F_{(1,22)} = 0.310$, $p = 0.583$), indicating that the increased coupled activation of DRG neurons in *Smoc2*$^{-/-}$ mice induced by pinch was present in mice of both sexes. To study whether other nociceptive mechanical stimuli also could induce the coupled activation of DRG neurons, we applied the strong press stimuli to the hindpaw of *Smoc2*$^{-/-}$ and *Smoc2*$^{+/+}$ mice of both sexes. The calcium imaging results showed that loss of SMOC2 also led to the increased number of coupled activated DRG neurons and total activated DRG neurons in mice of both sexes which responded to strong press stimuli (Fig. 5*F*, $F_{(1,9)} = 0.356$, $p = 0.566$; male: 17.9 ± 0.5% for *Smoc2*$^{+/+}$ mice and 37.3 ± 4.6% for *Smoc2*$^{-/-}$ mice; female: 18.7 ± 1.7% for *Smoc2*$^{+/+}$ mice and 32.8 ± 1.0% for *Smoc2*$^{-/-}$ mice; Fig. 5*G*, $F_{(1,9)} = 0.218$, $p = 0.651$; male: 9.1 ± 0.3% for *Smoc2*$^{+/+}$ mice and 23.8 ± 3.8% for *Smoc2*$^{-/-}$ mice; female: 9.6 ± 0.8% for *Smoc2*$^{+/+}$ mice and 21.0 ± 1.4% for *Smoc2*$^{-/-}$ mice; Fig. 5*H*, $F_{(1,9)} = 0.063$, $p = 0.807$; male:

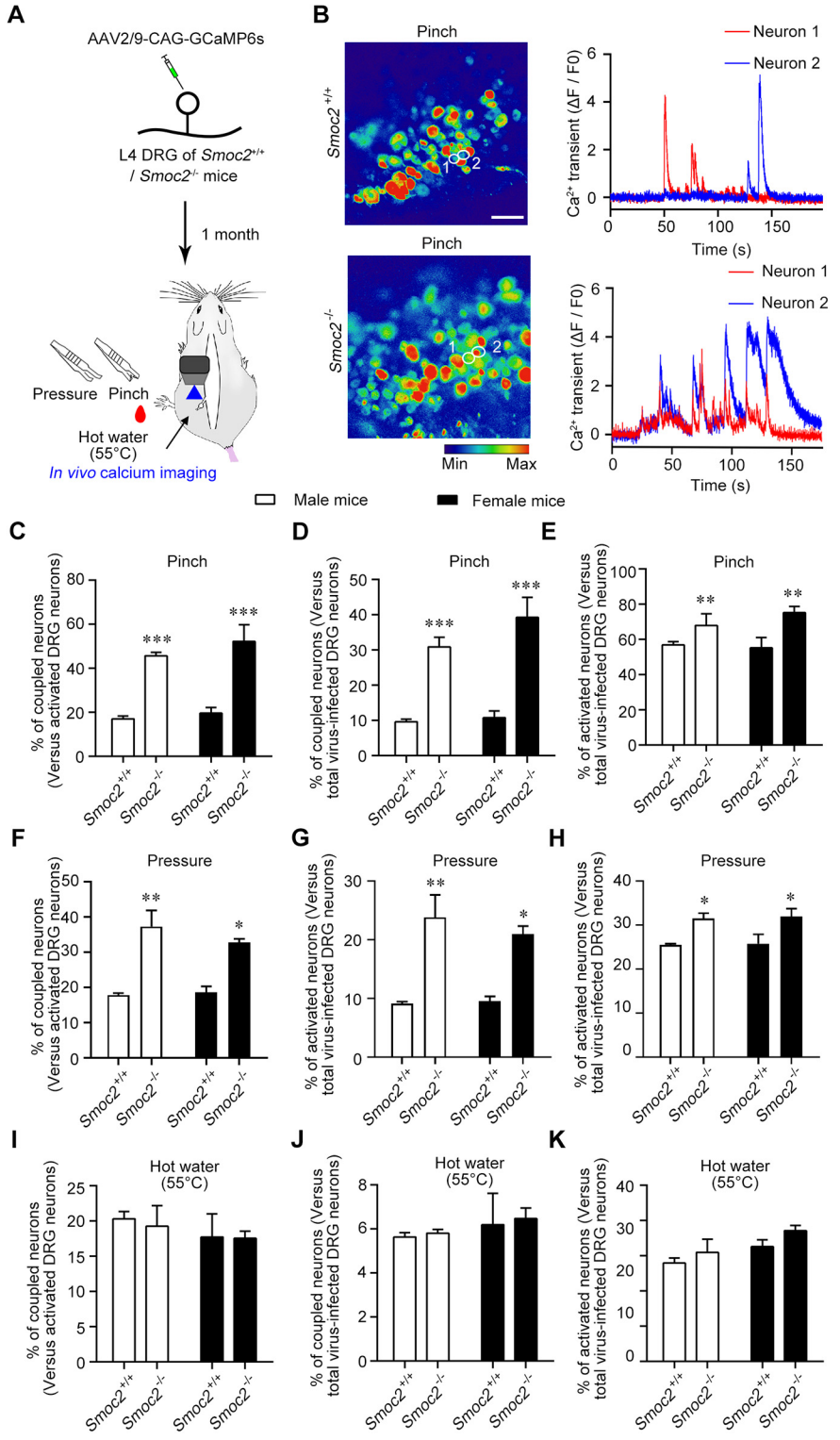

Figure 5. Loss of SMOC2 results in an increased coupled activation of adjacent DRG neurons induced by nociceptive mechanical stimuli. ***A***, Flowchart represents the procedure of *in vivo* DRG imaging. ***B***, Representative *in vivo* calcium images of L4 DRG neurons in $Smoc2^{+/+}$ mice and $Smoc2^{-/-}$ mice. The standard color palette varies from blue (minimal intensity of fluorescence) to red (maximum intensity of fluorescence). The time courses are shown for calcium transient evoked by pinch at the hindpaw of $Smoc2^{+/+}$ mice and $Smoc2^{-/-}$ mice. Each trace represents a single DRG neuron activated by pinch stimuli. All data of calcium transient are expressed as the percentage of baseline calcium transient (ΔF/F0). Scale bar, 50 μm. ***C***, Quantification of coupled neurons activated by pinch, normalized by total number of activated neurons by pinch in $Smoc2^{+/+}$ and $Smoc2^{-/-}$ mice. ***D***, Quantification of coupled neurons activated by pinch, normalized by total number of virus-infected DRG neurons in $Smoc2^{+/+}$ and $Smoc2^{-/-}$ mice. ***E***, Quantification of activated neurons by pinch, normalized by total number of virus-infected DRG neurons in $Smoc2^{+/+}$ and $Smoc2^{-/-}$ mice. $n = 7$ for male $Smoc2^{+/+}$ mice and $n = 6$ for male $Smoc2^{-/-}$ mice in ***C-E***. $n = 6$ for female $Smoc2^{+/+}$ mice and $n = 7$ for female $Smoc2^{-/-}$ mice in ***C-E***. ***F***, Quantification of coupled neurons activated by strong pressure, normalized by total number of activated neurons by strong pressure in $Smoc2^{+/+}$ and $Smoc2^{-/-}$ mice of both sexes. ***G***, Quantification of coupled neurons activated by strong pressure, normalized by total number of virus-infected DRG neurons in $Smoc2^{+/+}$ and $Smoc2^{-/-}$ mice of both sexes. ***H***, Quantification of activated neurons by strong pressure, normalized by total number of virus-infected DRG neurons in $Smoc2^{+/+}$ and $Smoc2^{-/-}$ mice of both sexes. $n = 3$ for male $Smoc2^{+/+}$ mice and $n = 4$ for male $Smoc2^{-/-}$ mice in ***F-H***. $n = 3$ for both female $Smoc2^{+/+}$ mice and $Smoc2^{-/-}$ mice in ***F-H***. ***I***, Quantification of coupled neurons activated by hot water (55°C), normalized by total number of activated neurons by hot water in $Smoc2^{+/+}$ and $Smoc2^{-/-}$ mice. ***J***, ***K***, Quantification of coupled neurons (***J***) and activated neurons (***K***) activated by hot water, normalized by total number of virus-infected DRG neurons in $Smoc2^{+/+}$ and $Smoc2^{-/-}$ mice. $n = 5$ for both male $Smoc2^{+/+}$ mice and $Smoc2^{-/-}$ mice in ***F-H***. $n = 4$ for female $Smoc2^{+/+}$ mice and $n = 6$ for female $Smoc2^{-/-}$ mice in ***I-K***. Data are mean ± SEM. $^{*}p < 0.05$, $^{**}p < 0.01$, $^{***}p < 0.001$ versus $Smoc2^{+/+}$ mice (two-way ANOVA with Bonferroni correction).

51.1 ± 0.5% for $Smoc2^{+/+}$ mice and 63.0 ± 2.5% for $Smoc2^{-/-}$ mice; female: 51.6 ± 4.2% for $Smoc2^{+/+}$ mice and 63.9 ± 3.5% for $Smoc2^{-/-}$ mice) (Fig. 5*F–H*). As a control, the percentage of coupled neurons in respond to 55°C hot water in the DRG of $Smoc2^{-/-}$ mice was similar to that of $Smoc2^{+/+}$ mice in both sexes (Fig. 5*I–K*). Thus, loss of SMOC2 causes an increased coupled activation of adjacent DRG neurons responding to nociceptive mechanical stimuli other than noxious heat stimuli in the DRG.

To further determine the vital role of SMOC2 in coupled neuronal activation induced by peripheral nociceptive mechanical stimuli, we injected SMOC2 protein into the DRG of $Smoc2^{-/-}$ mice and examined the effect of exogenous SMOC2 (Fig. 6*A*). *In vivo* calcium imaging showed that many simultaneously activated neurons adjacent to each other were decoupled 30 min after the injection of SMOC2 (Fig. 6*B*). Quantitative data showed that ~60% of coupled activated neurons were decoupled in $Smoc2^{-/-}$ mice after SMOC2 application (43.7 ± 2.6% and 17.5 ± 2.0% for before and after SMOC2 injection, $t = 10.77$, $df = 8$, $p < 0.001$) (Fig. 6*C*). The percentage of total virus-infected neurons with coupled activation in $Smoc2^{-/-}$ mice decreased from 30.5 ± 2.6% to 8.2 ± 1.8% after SMOC2 application ($t = 20.64$, $df = 8$, $p < 0.001$) (Fig. 6*D*). Moreover, the percentage of total activated neurons responding to nociceptive mechanical stimuli was also decreased significantly

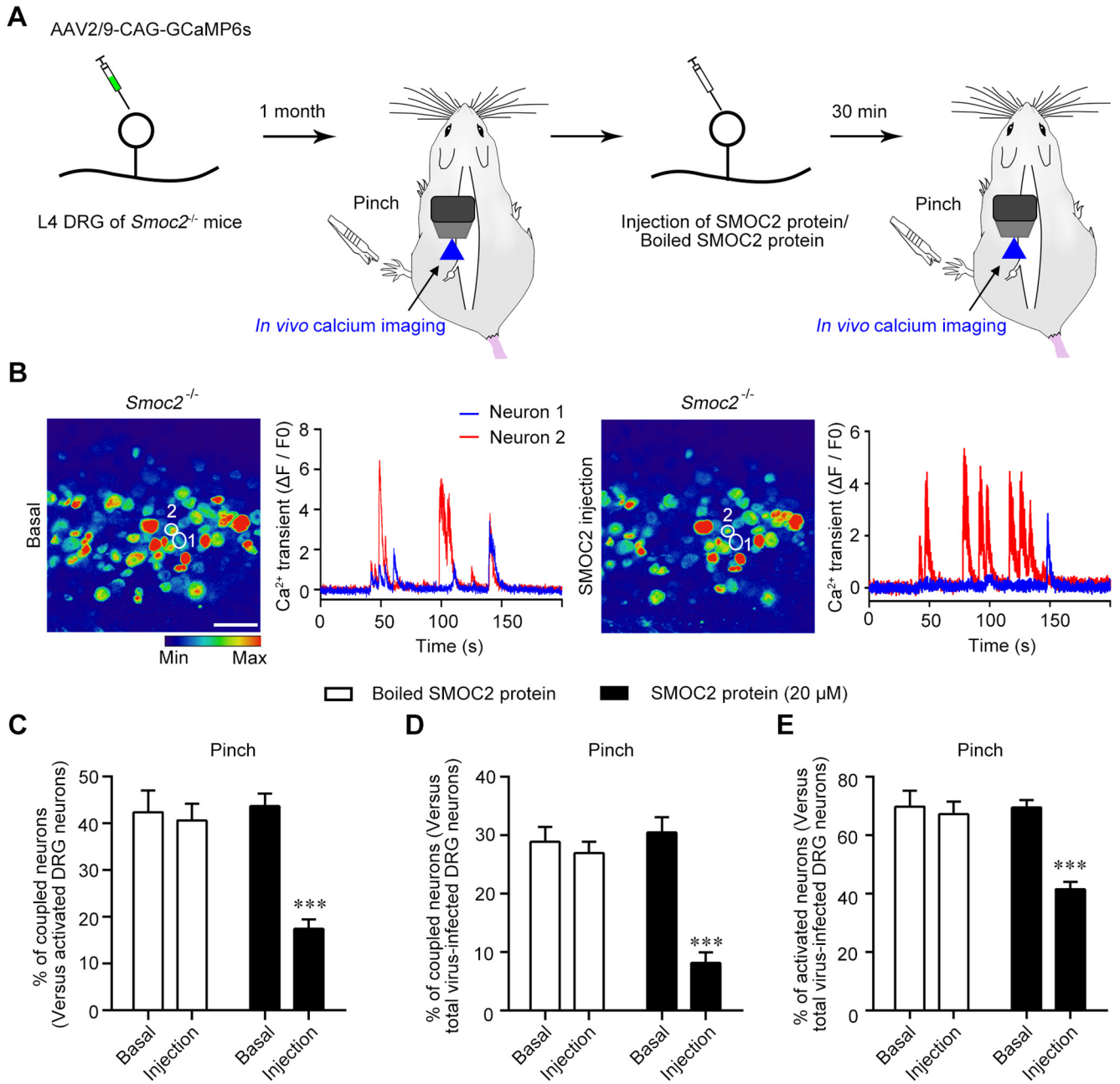

Figure 6. Application of SMOC2 suppresses the increased coupling of activated neurons by nociceptive mechanical stimuli in *Smoc2*$^{-/-}$ mice. ***A***, Flowchart represents the procedure of *in vivo* DRG imaging for protein injection. ***B***, Representative *in vivo* calcium images of L4 DRG neurons and calcium transient traces of the same two adjacent DRG neurons evoked by pinch at the hindpaw of *Smoc2*$^{-/-}$ mice before (Basal) and after injection of 20 μM SMOC2 protein. The standard color palette varies from blue (minimal intensity of fluorescence) to red (maximum intensity of fluorescence). All data of calcium transient are expressed as the percentage of baseline calcium transient (ΔF/F0). Scale bar, 50 μm. ***C***, Quantification of coupled neurons activated by pinch, normalized by total number of neurons activated by pinch in *Smoc2*$^{-/-}$ mice before (Basal) and after injection of SMOC2 or boiled SMOC2 protein. ***D***, ***E***, Quantification of coupled neurons (***D***) and activated neurons (***E***) activated by pinch, normalized by total number of virus-infected DRG neurons in *Smoc2*$^{-/-}$ mice before (Basal) and after injection of SMOC2 or boiled SMOC2 protein. $n = 5$ for two groups in ***C-E***. Data are mean ± SEM. ***$p < 0.001$ versus basal (two-way ANOVA with Bonferroni correction).

after SMOC2 application (69.5 ± 2.6% and 41.6 ± 2.4% for before and after SMOC2 injection, $t = 9.611$, df = 8, $p < 0.001$) (Fig. 6*E*). However, injection of boiled SMOC2 into the DRG of *Smoc2*$^{-/-}$ mice had no effect on the percentage of both coupled activated neurons and total activated neurons (Fig. 6*C*, $F_{(1,8)} = 6.109$, $p = 0.039$; Fig. 6*D*, $F_{(1,8)} = 7.679$, $p = 0.024$; Fig. 6*E*, $F_{(1,8)} = 6.495$, $p = 0.034$) (Fig. 6*C–E*). Notably, an increase of coupled neuronal activation in the DRG induced by nociceptive mechanical stimuli was because of loss of SMOC2. Together, these data suggest that fibroblast-secreted SMOC2 is required for inhibiting coupled activation of adjacent DRG neurons induced by nociceptive mechanical stimuli.

SMOC2 interacts with satellite glial P2X7R and inhibits the ATP-induced activation of P2X7R

We further explored the mechanism underlying the regulation of SMOC2 on coupled activation of DRG neurons. Previous studies showed that SGCs communicate with other cells or their enveloped neurons through gap junction or chemicals (Huang et al., 2013; Fan et al., 2019; Spray and Hanani, 2019). At first, we

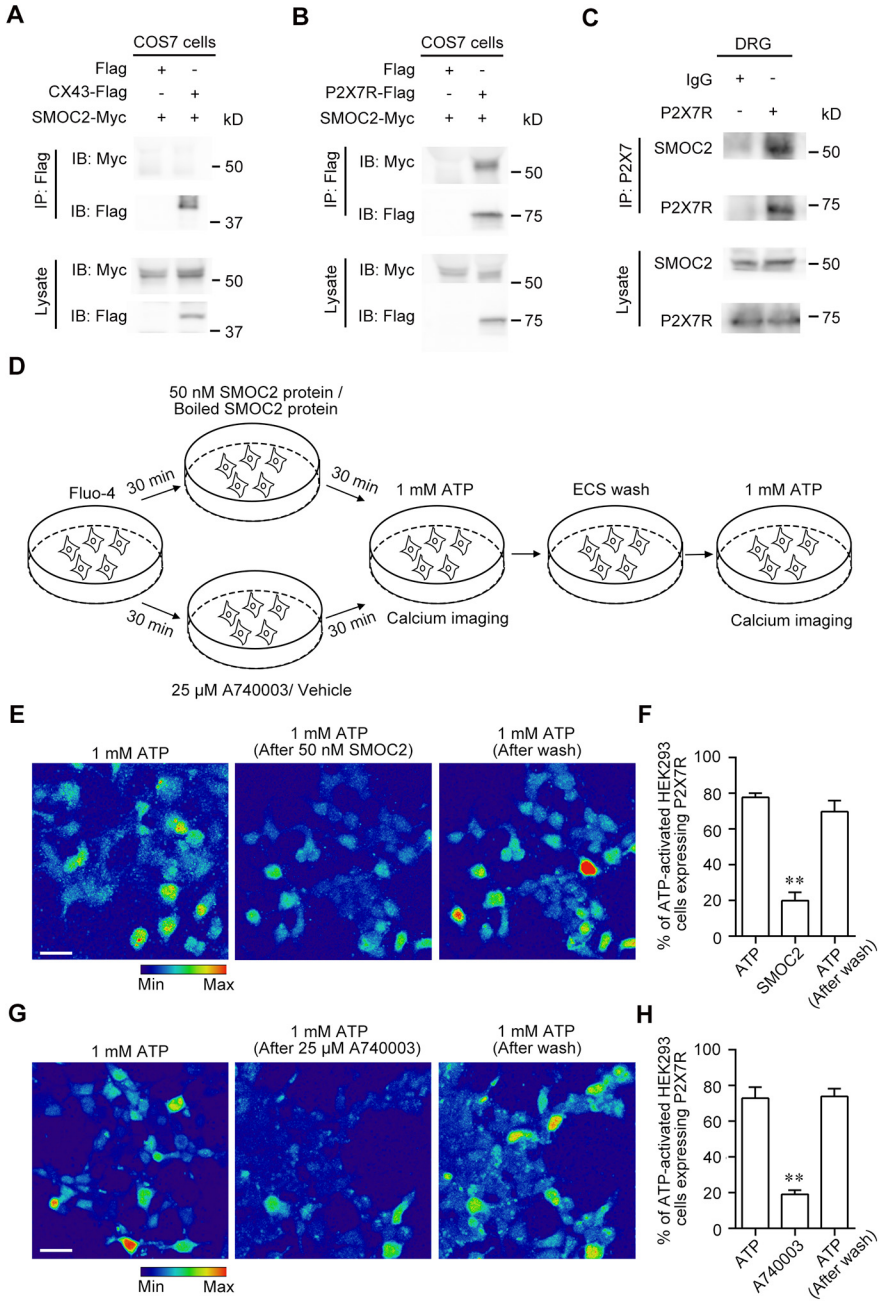

Figure 7. SMOC2 interacts with P2X7R receptor in the DRG and inhibits the activity of P2X7R. ***A***, Coimmunoprecipitation showing that SMOC2 did not interact with CX43 in COS7 cells coexpressing CX43-Flag and SMOC2-Myc ($n = 3$). ***B***, Coimmunoprecipitation showing that SMOC2 interacted with P2X7R in COS7 cells coexpressing P2X7R-Flag and SMOC2-Myc ($n = 3$). ***C***, Coimmunoprecipitation showing that SMOC2 interacted with P2X7R in DRGs ($n = 3$). ***D***, Flowchart represents the procedure of calcium imaging for ATP-induced activity in HEK293 cells expressing P2X7R after incubation with 25 μM A740003 or 50 nM SMOC2 protein for 30 min. ***E***, ***F***, Representative calcium images (***E***) and quantitative data (***F***) ($n = 3$) of ATP-induced activity in HEK293 cells expressing P2X7R before and after incubation with 50 nM SMOC2 protein. ***G***, ***H***, Representative calcium images (***G***) and quantitative data (***H***) ($n = 3$) of ATP-induced activity in HEK293 cells expressing P2X7R before and after incubation with 25 μM A740003. The standard color palette varies from blue (minimal intensity of fluorescence) to red (maximum intensity of fluorescence). All data of calcium transient are expressed as the percentage of baseline calcium transient ($\Delta F/F0$). Scale bar, 20 μm. Data are mean ± SEM. $^{**}p < 0.01$ versus ATP (one-way ANOVA with Dunnett correction).

examined whether SMOC2 could interact with CX43, an important component of gap junction in SGCs (Garrett and Durham, 2008; Kim et al., 2016). Coimmunoprecipitation showed that SMOC2 did not interact with CX43 in COS7 cells (Fig. 7*A*), implying that the gap junction formed by CX43 in SGCs does not mediate the effect of SMOC2. As previous work reported, the activation of purinergic receptors through transmitters, most notably ATP, is a common way for neurons to communicate with other cells or neurons (Huang et al., 2013; Diezmos et al., 2016). Purinergic receptor P2X7 is known to be exclusively expressed in SGCs (Y. Chen et al., 2008; L. Chen et al., 2016), and activation of this receptor contributes to nociceptive behaviors, especially mechanical allodynia after peripheral inflammation, by regulating the communication between DRG neurons and their attached SGCs (Chessell et al., 2005; Sorge et al., 2012). Therefore, we examined the possibility that SMOC2 regulated the communication among adjacent DRG neurons by interacting with satellite glial P2X7R. Coimmunoprecipitation detected the interaction between SMOC2 and P2X7R both in COS7 cells exogenously coexpressing SMOC2-Myc and P2X7R-Flag (Fig. 7*B*) and in the lysate of mouse DRGs (Fig. 7*C*), providing a molecular basis for the SMOC2/P2X7R interaction. Further, calcium imaging in HEK293 cells expressing P2X7R-mCherry showed that the inward Ca^{2+} current induced by ATP was significantly inhibited by SMOC2 ($F_{(2,6)} = 37.590$, $p = 0.003$; ATP: 77.7 ± 4.1%, SMOC2: 19.9 ± 8.0%, wash ATP: 69.7 ± 6.2%, 103 cells) (Fig. 7*D–F*). Similar effects were observed by application of A740003, a specific antagonist of P2X7R ($F_{(2,4)} = 34.96$, $p = 0.003$; ATP: 72.8 ± 6.3%, SMOC2: 19.2 ± 3.9%, wash ATP: 73.9 ± 4.3%, 126 cells) (Fig. 7*G*,*H*). These results indicate that SMOC2 inhibits the activation of P2X7R evoked by ATP.

SMOC2 regulates the coupling of activated neurons by inhibiting satellite glial P2X7R

We then investigated whether SMOC2 participated in the P2X7R-mediated regulation of neuronal coupling. We directly injected A740003 into the L4 DRG of *Smoc2*$^{-/-}$ mice (Fig. 8*A*). The calcium imaging showed that inhibition of P2X7R with A740003 attenuated the coupling of activated neurons in *Smoc2*$^{-/-}$ mice (Fig. 8*B*). The coupled percentage of activated neurons induced by nociceptive mechanical stimuli were dropped from 38.9 ± 1.4% to 17.9 ± 3.2% after the injection of A740003 to the DRG ($F_{(1,\ 7)} = 23.260$, $p = 0.002$; A740003 injection: $t = 6.122$, df = 7, $p = 0.001$) (Fig. 8*C*). Meanwhile, the percentage of total virus-infected neurons with coupled activation was dropped from 26.4 ± 2.3% to 6.8 ± 1.3% after the injection of A740003 to the DRG ($F_{(1,\ 7)} = 13.61$, $p = 0.008$; A740003 injection: $t = 10.14$, df = 7, $p < 0.001$) (Fig. 8*D*). The total activated neurons were also decreased

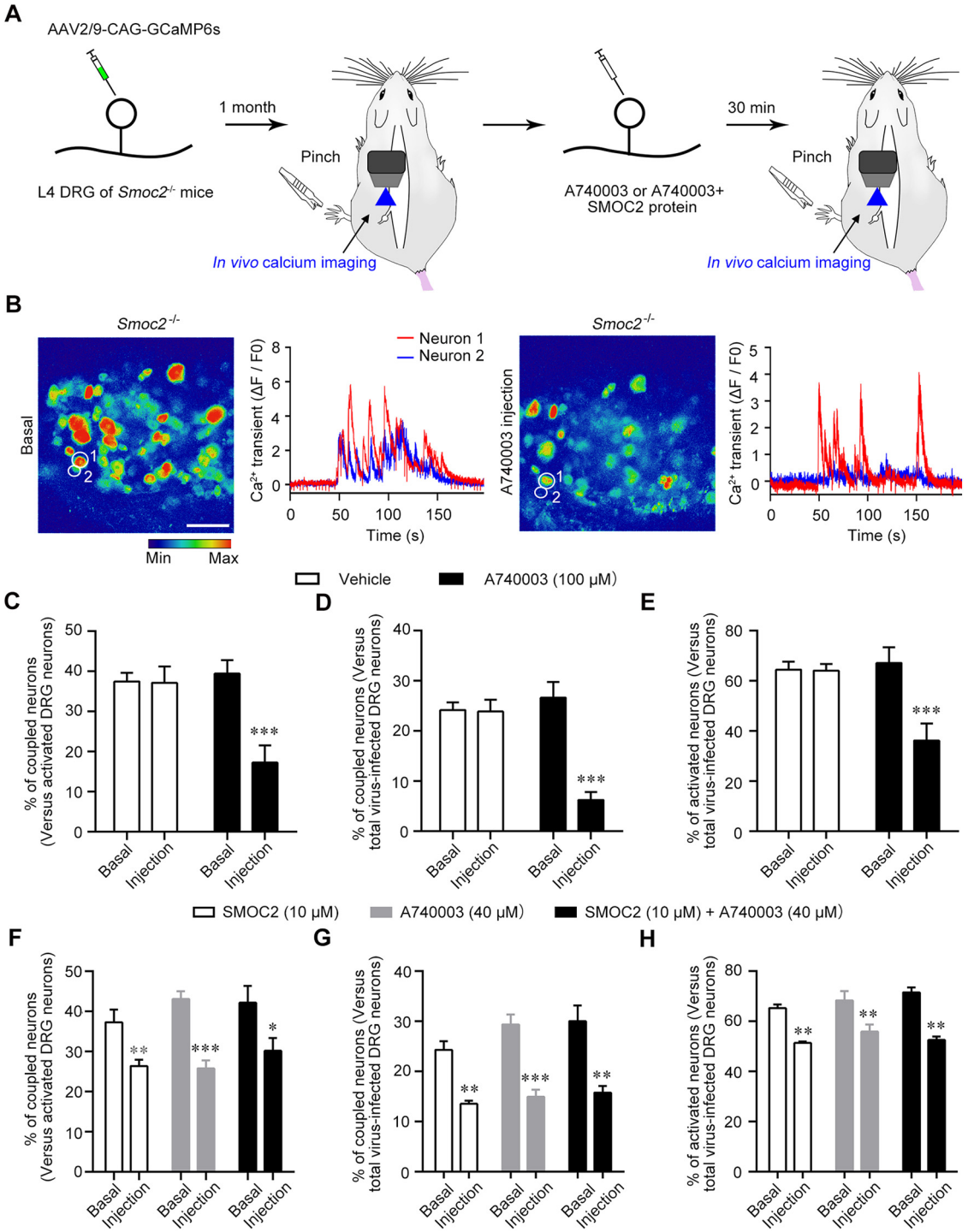

Figure 8. SMOC2 regulates coupled activation of DRG neurons through P2X7R. ***A***, Flowchart represents the procedure of *in vivo* DRG imaging for A740003 injection or the coinjection of A740003 and SMOC2 protein. ***B***, Representative *in vivo* calcium images of L4 DRG neurons and calcium transient traces of the same two adjacent DRG neurons evoked by pinch at the hindpaw of $Smoc2^{-/-}$ mice before (Basal) and after 100 μM A740003 injection. The standard color palette varies from blue (minimal intensity of fluorescence) to red (maximum intensity of fluorescence). All data of calcium transient are expressed as the percentage of baseline calcium transient ($\Delta F/F0$). Scale bar, 50 μm. ***C***, Quantification of coupled neurons activated by pinch, normalized by total number of neurons activated by pinch in $Smoc2^{-/-}$ mice before (Basal) and after injection of 100 μM A740003 or vehicle. ***D***, ***E***, Quantification of coupled neurons (***D***) and activated neurons (***E***) activated by pinch, normalized by total number of virus-infected DRG neurons in $Smoc2^{-/-}$ mice before (Basal) and after injection of 100 μM A740003 or vehicle. $n = 4$ for A740003 injection and $n = 3$ for vehicle injection in ***C-E***. ***F***, Quantification of coupled neurons activated by pinch, normalized by total number of neurons activated by pinch in $Smoc2^{-/-}$ mice before (Basal) and after injection of 10 μM SMOC2 protein, 40 μM A740003, or coinjection of 10 μM SMOC2 protein and 40 μM A740003. ***G***, ***H***, Quantification of coupled neurons (***G***) and activated neurons (***H***) activated by pinch, normalized by total number of virus-infected DRG neurons in $Smoc2^{-/-}$ mice before (Basal) and after injection of 10 μM SMOC2 protein, 40 μM A740003, or coinjection of 10 μM SMOC2 protein and 40 μM A740003. $n = 4$ for SMOC2 injection, $n = 5$ for A740003 injection, and $n = 3$ for coinjection of SMOC2 protein and A740003 in ***F-H***. Data are mean ± SEM. *$p < 0.05$, **$p < 0.01$ versus basal (two-way ANOVA with Bonferroni correction).

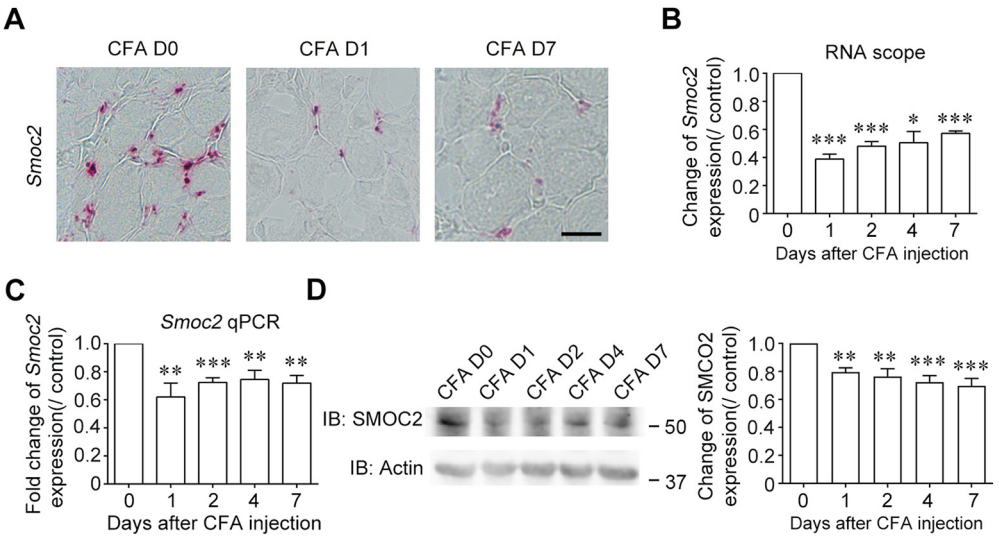

Figure 9. Peripheral inflammation causes the decreased expression of SMOC2 in the DRG. ***A***, ***B***, Representative images (***A***) and quantitative data (***B***) of RNAscope showing that the expression of *Smoc2* in the DRG was decreased in mice after peripheral CFA injection ($n = 3$). ***C***, qPCR showing that the expression of *Smoc2* was reduced in the DRG of mice after peripheral CFA injection ($n = 5$). ***D***, Immunoblotting showing that the expression of SMOC2 was reduced in the DRG of mice after peripheral CFA injection ($n = 5$). Scale bar, 20 μm. Data are mean ± SEM. $^*p < 0.05$, $^{**}p < 0.01$, $^{***}p < 0.001$ versus day 0 (one-way ANOVA with Dunnett correction).

after A740003 injection (67.6 ± 4.4% for before and 33.4 ± 4.1% for after; $F_{(1, 7)} = 7.984$, $p = 0.023$; A740003 injection: $t = 30.13$, df = 7, $p < 0.001$) (Fig. 8*E*). Moreover, we examined whether SMOC2 could further affect the A740003-inhibited coupling of activated neurons. We coinjected SMOC2 and A740003 both in a much lower concentration. The inhibition of activated coupling neurons induced by nociceptive mechanical stimuli was not enhanced by coinjection of SMOC2 and A740003 compared with application of SMOC2 or A740003 alone ($F_{(2, 9)} = 0.908$, $p = 0.438$; SMOC2, 37.3 ± 3.1% for before and 26.4 ± 1.6% for after, $t = 3.962$, df = 9, $p = 0.01$; A740003, 43.1 ± 2.0% for before and 25.8 ± 2.0% for after, $t = 7.013$. df = 9, $p < 0.001$; coinjection, 42.2 ± 4.2% for before and 30.2 ± 3.2% for after, $t = 3.766$, df = 9, $p = 0.013$) (Fig. 8*F*). The effect on inhibiting the coupled activation of total virus-infected neurons by coinjection of SMOC2 and A740003 was similar to that by application of SMOC2 or A740003 alone ($F_{(2, 9)} = 2.375$, $p = 0.149$. SMOC2, 24.3 ± 1.7% for before and 13.5 ± 0.7% for after, $t = 4.850$, df = 9, $p = 0.003$; A740003: 29.8 ± 1.5% for before and 13.8 ± 1.6% for after, $t = 8.046$, df = 9, $p < 0.001$; coinjection: 30.0 ± 3.1% for before and 15.8 ± 1.3% for after, $t = 5.562$, df = 9, $p = 0.001$) (Fig. 8*G*). The percentage of total activated neurons was not different among application of SMOC2 or A740003 alone, and coinjection ($F_{(2, 9)} = 1.126$, $p = 0.366$; SMOC2, 65.3 ± 1.5% for before and 51.4 ± 0.6% for after, $t = 4.020$, df = 9, $p = 0.009$; A740003, 70.0 ± 3.6% for before and 52.7 ± 2.5% for after, $t = 5.574$, df = 9, $p = 0.001$; coinjection, 71.6 ± 1.9% for before and 52.6 ± 1.4% for after, $t = 4.743$, df = 9, $p = 0.003$) (Fig. 8*H*). These results imply that SMOC2 and P2X7R are in the same pathway of regulating neuronal coupling. Since SMOC2 interacted with P2X7R and inhibited the ATP-induced activation of P2X7R, we speculated that satellite glial P2X7R was the downstream target of fibroblastic SMOC2 in the regulation of neuronal coupling in the DRG. Together, these data suggest that fibroblast-secreted SMOC2 regulates the coupled activation of adjacent DRG neurons responded to nociceptive mechanical stimuli by affecting satellite glial P2X7R.

Peripheral inflammation results in a decrease of SMOC2 and an increase of neuronal coupling

The communication of adjacent DRG neurons is increased following peripheral tissue injury (Song et al., 2014; Kim et al., 2016). Since loss of SMOC2 led to the increased coupled activation of adjacent DRG neurons, we examined the change of SMOC2 expression under pathologic conditions, which may contribute to the changed communication of adjacent neurons. We first examined the expression of SMOC2 in mouse DRGs after peripheral inflammation induced by complete Freund's adjuvant (CFA). RNAscope showed that the number of *Smoc2*$^+$ puncta around DRG neurons was decreased in the CFA model ($F_{(4, 10)} = 29.77$, $p < 0.001$) (Fig. 9*A*,*B*). qPCR detected that the level of *Smoc2* mRNA in the DRG was also decreased after peripheral inflammation ($F_{(4, 20)} = 4.535$, $p = 0.009$) (Fig. 9*C*). Then, we further investigated the change of SMOC2 protein in mouse DRG after CFA plantar injection. Consistently, immunoblotting result showed that CFA-induced reduction in *Smoc2* mRNA resulted in a decrease in the SMOC2 protein level ($F_{(4, 20)} = 8.273$, $p < 0.001$) (Fig. 9*D*).

Double immunostaining with SMOC2 and FABP7 showed that the expression of SMOC2 among the adjacent clustered DRG neurons was decreased after inflammation, while as a control, the expression of FABP7 was unchanged (Fig. 10*A*). The statistical result showed that the fluorescence intensity of SMOC2 in the DRG was decreased after inflammation and that of FABP7 was not changed (FABP7: $F_{(2, 30)} = 0.153$, $p = 0.861$; SMOC2: $F_{(2, 6)} = 171.000$, $p < 0.001$) (Fig. 10*B*). Moreover, we want to know whether the decrease of SMOC2 led to the increased clustered neurons in the CFA model. Double immunostaining with SMOC2 and Collagen IV showed that the percentage of clustered neurons in the DRG after inflammation was increased compared with control mice ($F_{(4, 13)} = 66.570$, $p < 0.001$) (Fig. 10*B*,*C*), implying that the decreased expression of SMOC2 may contribute to the increased clustered neurons. Since SMOC2 was expressed and secreted by fibroblasts in the DRG, we examined the change of fibroblasts in the DRG after peripheral inflammation. Double immunostaining with PDGFRα and SMOC2 showed that adjacent DRG neurons were obstructed by PDGFRα^+ fibroblasts and

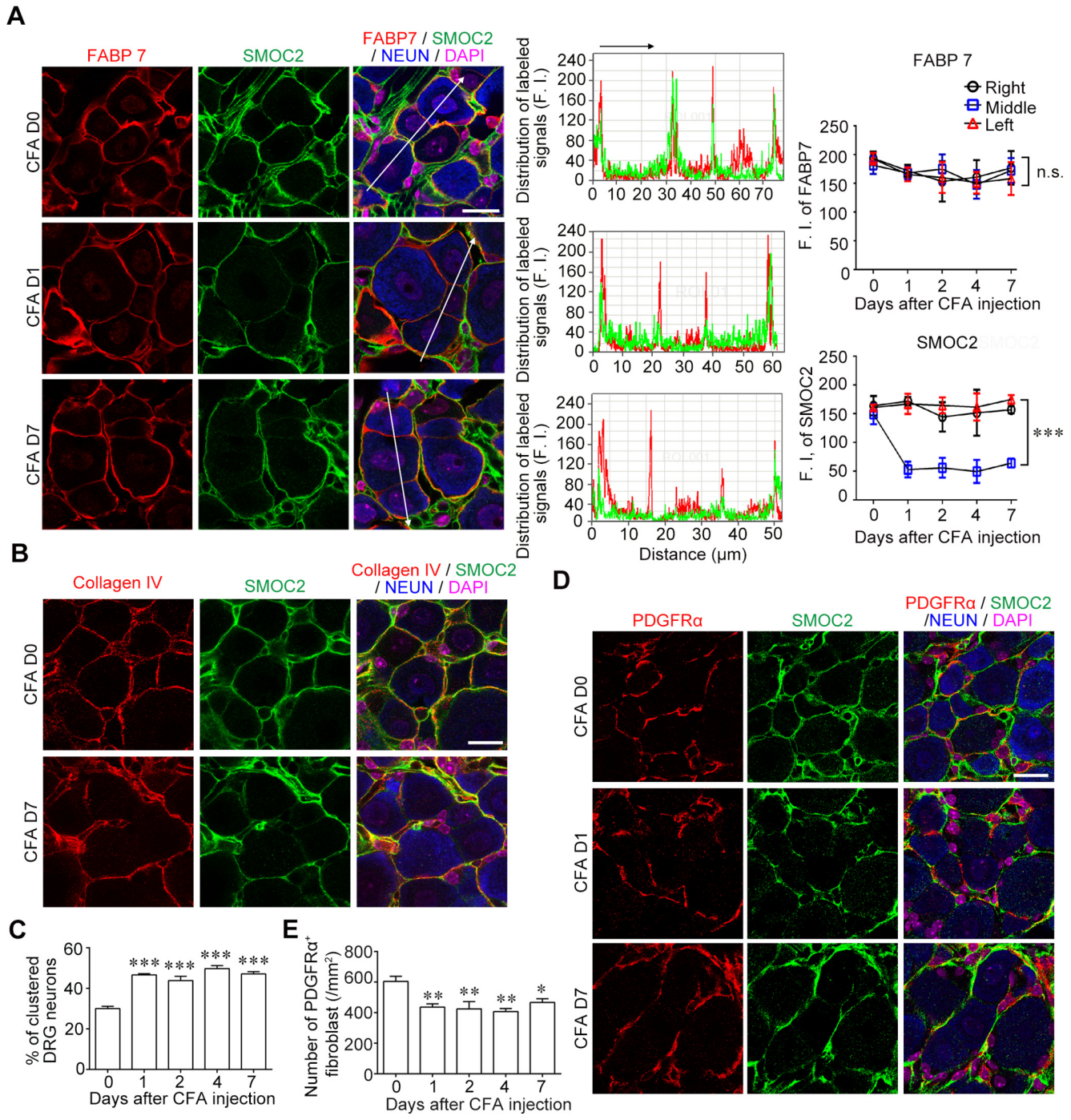

Figure 10. Peripheral inflammation causes a decrease of fibroblasts and an increase of neuronal clusters. ***A***, Representative images of immunostaining (left) and the corresponding quantitative data showing that the expression of SMOC2 was decreased (middle, green; right bottom) and the presence of FABP7$^+$ SGCs was not changed (middle, red; right top) among adjacent DRG neurons in mice after CFA injection ($n = 3$). ***B***, ***C***, Representative images of immunostaining (***B***) and quantitative data (***C***) showing that the expression of both SMOC2 (green) and Collagen IV (red) among adjacent DRG neurons was decreased, and the percentage of clustered neurons in the DRG was increased in mice after CFA injection ($n = 3$). ***D***, ***E***, Representative images of immunostaining (***D***) and quantitative data (***E***) showing that the number of PDGFRα^+ fibroblasts per square millimeter of DRG soma was decreased in mice after CFA injection ($n = 3$). Scale bar, 20 μm. Data are mean ± SEM. *$p < 0.05$, **$p < 0.01$, ***$p < 0.001$ versus day 0, two-way ANOVA with Bonferroni correction (***A***) and one-way ANOVA with Dunnett correction (***C***,***E***).

SMOC2 in control mice. However, in CFA-injected mice, the number of PDGFRα^+ fibroblasts in the DRG neurons was decreased ($F_{(4,\ 14)} = 6.058$, $p = 0.005$) (Fig. 10*D*,*E*). Therefore, peripheral inflammation causes a decrease of fibroblast-derived SMOC2, and an increase of neuronal clusters in the DRG.

Considering the increased clusters of DRG neurons in CFA-induced mice and the regulation of SMOC2 to coupled activation of neurons, we hypothesized that application of exogenous SMOC2 could reverse the increased coupled activation of adjacent DRG neurons after peripheral inflammation. With the application of nociceptive mechanical stimuli to the hindpaw of mice 7 d after CFA injection, the coupled percentage of activated neurons was largely increased compared with the control mice (Figs. 5*C* and 11*A*,*B*), which was consistent with the previous report (Kim et al., 2016). After injection of SMOC2 into L4 and L5 DRGs for 30 min, the coupling of neuronal activation was

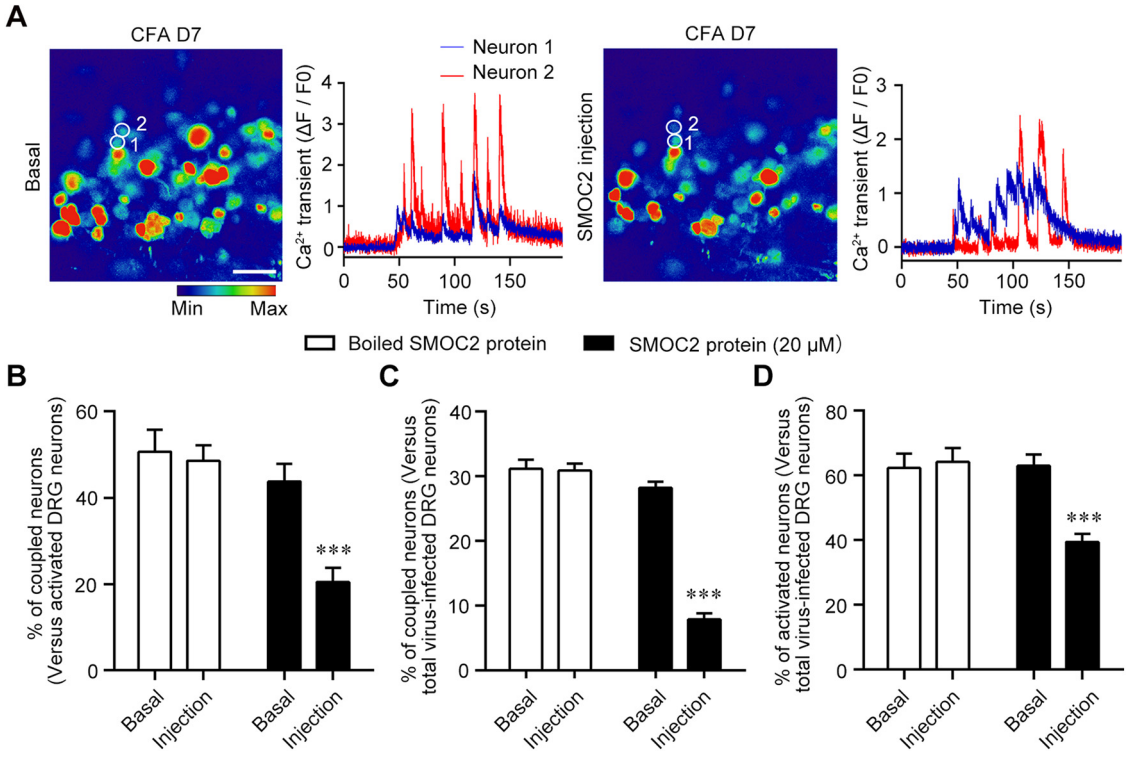

Figure 11. Application of SMOC2 inhibits the coupled activation of DRG neurons after peripheral inflammation. ***A***, Representative *in vivo* calcium images of L4 DRG neurons and calcium transient traces of the same two adjacent DRG neurons evoked by pinch at the hindpaw of mice 7 d after peripheral CFA injection. The standard color palette varies from blue (minimal intensity of fluorescence) to red (maximum intensity of fluorescence). All data of calcium transient are expressed as the percentage of baseline calcium transient (ΔF/F0). Scale bar, 50 μm. ***B***, Quantification of coupled neurons activated by pinch, normalized by total number of neurons activated by pinch in mice 7 d after CFA injection before (Basal) and after injection of SMOC2 or boiled SMOC2 protein. ***C***, ***D***, Quantification of coupled neurons (***C***) and activated neurons (***D***) activated by pinch, normalized by total number of virus-infected DRG neurons in mice 7 d after CFA injection before (Basal) and after injection of SMOC2 or boiled SMOC2 protein. Data are mean ± SEM; $n = 4$. ***$p < 0.001$ versus basal (two-way ANOVA with Bonferroni correction).

significantly inhibited. Only 20.5 ± 3.2% of activated neurons were coupled after SMOC2 injection compared with 43.8 ± 4.1% in basal condition ($F_{(1, 6)} = 11.170$, $p = 0.016$; SMOC2 injection: $t = 11.470$, df = 6, $p < 0.001$) (Fig. 11*B*). The percentage of total virus-infected neurons with coupled activation was dropped from 28.2 ± 0.9% to 7.9 ± 0.9% after SMOC2 injection ($F_{(1, 6)} = 74.250$, $p < 0.001$; SMOC2 injection: $t = 20.740$, df = 6, $p < 0.001$) (Fig. 11*C*). The percentage of total activated neurons induced by nociceptive mechanical stimuli was also dropped from 63.0 ± 3.5% to 39.5 ± 2.4% after the application of SMOC2 to the DRG of CFA mice ($F_{(1, 6)} = 7.975$, $p = 0.030$; SMOC2 injection: $t = 12.170$, df = 6, $p < 0.001$) (Fig. 11*D*). These results suggest that SMOC2 regulates the coupled activation of DRG neurons induced by noxious mechanical stimuli after peripheral inflammation.

Discussion

DRG neurons detect peripheral somatosensory stimuli, and their soma is surrounded by SGCs and fibroblasts. In the present study, we reveal that SMOC2 is specifically expressed in fibroblasts, and secreted to become a component of the basement membrane and inhibit satellite glial P2X7R in the DRG. SMOC2 deficiency increases neuronal clusters and further enhances coupled activation of adjacent DRG neurons through the disinhibition of P2X7R, which leads to mechanical allodynia other than heat hyperalgesia (Fig. 12). This study uncovers non-neuronal fibroblasts and their secreted molecules as critical modulators in pain sensation.

Fibroblast-secreted SMOC2 regulates mechanical nociception

In the present study, SMOC2 has been detected to be spontaneously secreted from cultured fibroblasts and tend to adhere to the cell membrane. In general, single DRG neuron is tightly enveloped by SGCs to form an independent functional unit. This unit consisted of a DRG neuron, and its attached SGCs are further surrounded by the basement membrane and fibroblasts. Fibroblast-derived SMOC2 is distributed within the basement membrane. Loss of SMOC2 disrupts the integrity of basement membrane and increases the number of neuronal clusters, which provides a possibility to affect the communication of adjacent neurons in the DRG. We noticed that most clustered DRG neurons are small or medium neurons in the DRG of both $Smoc2^{+/+}$ and $Smoc2^{-/-}$ mice. Traditionally, small or medium DRG neurons are related to the nociceptive transmission. However, the reason why loss of SMOC2 mainly leads to the disruption of basement membrane around small and medium DRGs neurons needs further study.

Previous reports highlight the role of DRG neurons and SGCs in nociceptive sensation (Li et al., 2011; Oliveira et al., 2017; Shin et al., 2020; Xie et al., 2020). Small DRG neurons expressing different ion channels and receptors are considered as sensors for noxious stimuli (Dhaka et al., 2006). SGCs regulate neuronal excitability and nociception through their receptors, ion channels, and gap junction (Huang et al., 2013). The present study provides functional evidences for the notion that fibroblast-secreted molecules in the DRG are involved in pain sensation. Fibroblast-secreted SMOC2 specifically

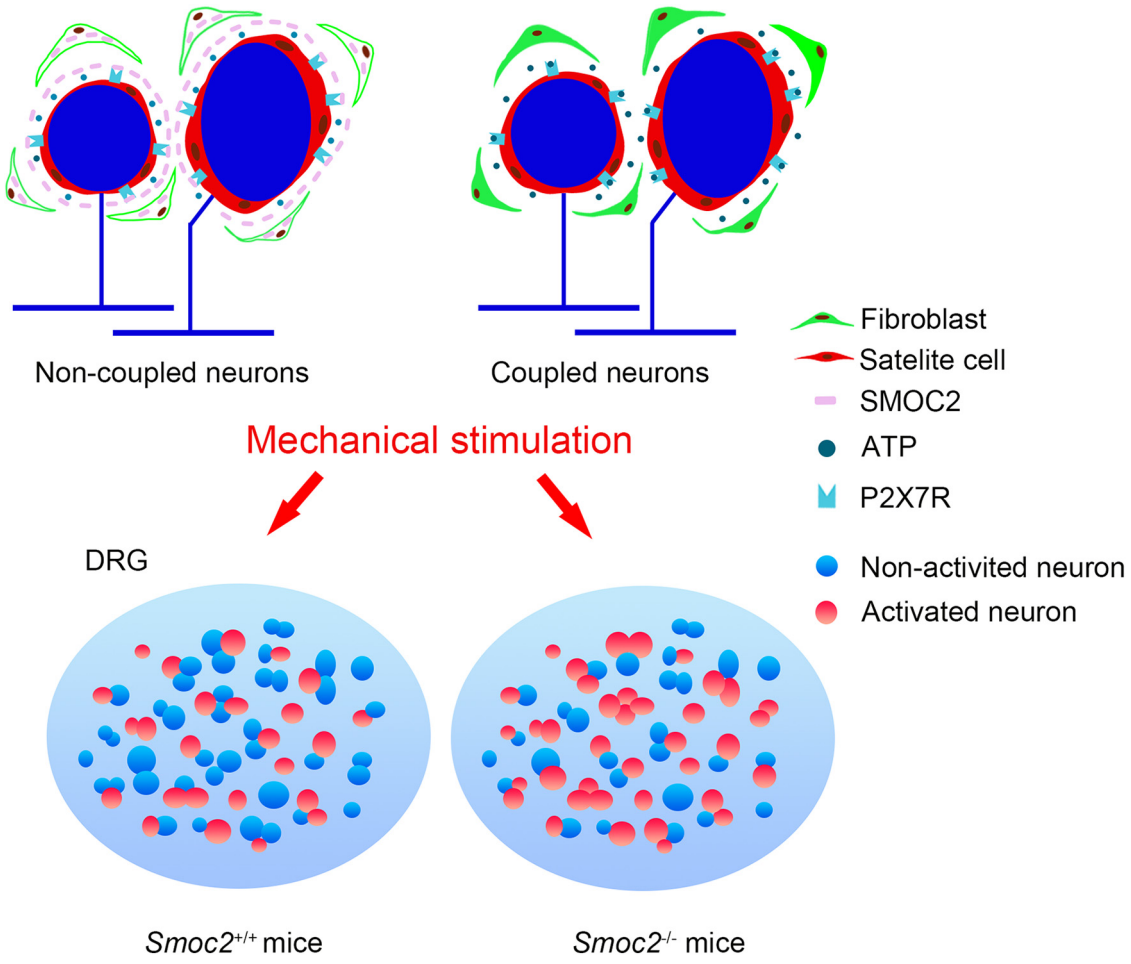

Figure 12. Proposed model for SMOC2 in regulating coupled activation of adjacent DRG neurons induced by noxious mechanical stimulation. SMOC2 is expressed and secreted in fibroblasts of the DRG. Fibroblastic SMOC2 prevents the communication of adjacent DRG neurons by inhibiting P2X7R in SGCs. The deficiency of SMOC2 increases the number of clustered neurons in the DRG, and elevates coupled activation of adjacent neurons induced by nociceptive mechanical stimuli through the disinhibition of satellite glial P2X7R.

affects the mechanical nociception. Loss of SMOC2 reduces the nociceptive mechanical threshold but does not affect other sensations, such as heat, chemical nociception, and itch. Fibroblasts are a kind of heterogeneous cell and play different roles according to their position under physiological and pathologic conditions. For example, the previous study reported that fibroblastic PI16 was expressed in the meninges of DRG other than within the DRG. The expression of PI16 in the meninges of DRG was increased and PI16 promoted neuropathic pain after nerve injury of mice (Singhmar et al., 2020). Our results showed that SMOC2 expressed in the fibroblasts within the DRG inhibits the mechanical nociception by inhibiting coupled activation of primary sensory neurons. Considering the exuberant secretion of fibroblasts, the molecules secreted by fibroblasts in the DRG may play vital roles in the regulation of multiple sensations, which is ignored before and needs to be further investigated.

SMOC2 suppresses coupled activation of adjacent DRG neurons through inhibiting P2X7R

Neuronal coupling in the DRG has been observed in the structure through dye injection of the individual DRG neuron (Huang et al., 2010; Blum et al., 2014; Hanani, 2015). A previous study reports that the coupled activation of adjacent DRG neurons contributes to the mechanical allodynia under pathologic pain condition through *in vivo* DRG calcium imaging (Kim et al., 2016). In the present study, immunostaining shows that the number of clustered DRG neurons is increased in *Smoc2*$^{-/-}$ mice. *In vivo* calcium imaging detects that loss of SMOC2 leads to an increased coupled activation of adjacent DRG neurons responded to nociceptive mechanical stimuli, which can be reversed by injection of SMOC2 into the DRG. These phenomena provide a mechanism that the molecule secreted from fibroblasts regulates coupled activation of adjacent DRG neurons.

Previous study reveals that adjacently neuronal communication in the DRG is mediated by the gap junction through CX43 (Huang et al., 2013). A direct effect on gap junction is excluded because SMOC2 does not interact with CX43 in the DRG in the present study. It is also known that satellite glial P2X7R mediates the communication between SGCs and DRG neurons (Chessell et al., 2005; Neves et al., 2020). The role of satellite glial P2X7R in neuronal coupling is proved by *in vivo* calcium imaging in *Smoc2*$^{-/-}$ mice, and SMOC2 is able to interact with P2X7 and block the ATP-induced Ca^{2+} transient of P2X7R. Coinjection of A740003 with SMOC2 to the DRG in *Smoc2*$^{-/-}$ mice does not display enhanced effect on the SMOC2-induced inhibition of neuronal coupling. These results imply that P2X7R is the downstream target of SMOC2. Since the instantaneous injection of SMOC2 into the DRG is not able to reconstitute the basement

membrane by loss of SMOC2, a direct inhibition of SMOC2 on satellite glial P2X7R may serve as a key linker to suppress the neuronal coupling.

SMOC2 is involved in mechanical allodynia after peripheral inflammation

The sensitization of DRG neurons under pathologic condition, such as peripheral inflammation, often leads to chronic pain (Li et al., 2011; Luo et al., 2018). The altered communication of neurons and SGCs in the DRG has been reported after peripheral inflammation (Blum et al., 2014; Hanani, 2015; Neves et al., 2020). In the present study, RNAscope, qPCR, and immunostaining show that SMOC2 is decreased in the DRG after peripheral inflammation with CFA injection. The anomaly of extracellular matrix is related to abnormal neuronal functions (Previtali et al., 2008). Peripheral inflammation also results in an increased number of clustered neurons. *In vivo* calcium imaging detects that application of SMOC2 to the DRG reverses the increased neuronal coupling induced by nociceptive mechanical stimuli after periphery inflammation. All this evidence supports that downregulation of SMOC2 in the DRG after peripheral inflammation may be an important mechanism to disinhibit neuronal coupling and induce persistent mechanical allodynia.

References

Basbaum AI, Bautista DM, Scherrer G, Julius D (2009) Cellular and molecular mechanisms of pain. Cell 139:267–284.

Blum E, Procacci P, Conte V, Hanani M (2014) Systemic inflammation alters satellite glial cell function and structure: a possible contribution to pain. Neuroscience 274:209–217.

Bolivar S, Navarro X, Udina E (2020) Schwann cell role in selectivity of nerve regeneration. Cells 9:2131.

Chen L, Liu YW, Yue K, Ru Q, Xiong Q, Ma BM, Tian X, Li CY (2016) Differential expression of ATP-gated P2X receptors in DRG between chronic neuropathic pain and visceralgia rat models. Purinergic Signal 12:79–87.

Chen Y, Zhang X, Wang C, Li G, Gu Y, Huang LY (2008) Activation of P2X7 receptors in glial satellite cells reduces pain through downregulation of P2X3 receptors in nociceptive neurons. Proc Natl Acad Sci USA 105:16773–16778.

Chessell IP, Hatcher JP, Bountra C, Michel AD, Hughes JP, Green P, Egerton J, Murfin M, Richardson J, Peck WL, Grahames CB, Casula MA, Yiangou Y, Birch R, Anand P, Buell GN (2005) Disruption of the P2X7 purinoceptor gene abolishes chronic inflammatory and neuropathic pain. Pain 114:386–396.

Dhaka A, Viswanath V, Patapoutian A (2006) Trp ion channels and temperature sensation. Annu Rev Neurosci 29:135–161.

Diezmos EF, Bertrand PP, Liu L (2016) Purinergic signaling in gut inflammation: the role of connexins and pannexins. Front Neurosci 10:311.

Dorrier CE, Aran D, Haenelt EA, Sheehy RN, Hoi KK, Pintaric L, Chen Y, Lizama CO, Cautivo KM, Weiner GA, Popko B, Fancy SP, Arnold TD, Daneman R (2021) CNS fibroblasts form a fibrotic scar in response to immune cell infiltration. Nat Neurosci 24:234–244.

Dublin P, Hanani M (2007) Satellite glial cells in sensory ganglia: their possible contribution to inflammatory pain. Brain Behav Immun 21:592–598.

Fan W, Zhu X, He Y, Zhu M, Wu Z, Huang F, He H (2019) The role of satellite glial cells in orofacial pain. J Neurosci Res 97:393–401.

Garrett FG, Durham PL (2008) Differential expression of connexins in trigeminal ganglion neurons and satellite glial cells in response to chronic or acute joint inflammation. Neuron Glia Biol 4:295–306.

Gerarduzzi C, Kumar RK, Trivedi P, Ajay AK, Iyer A, Boswell S, Hutchinson JN, Waikar SS, Vaidya VS (2017) Silencing SMOC2 ameliorates kidney fibrosis by inhibiting fibroblast to myofibroblast transformation. JCI Insight 2:e90299.

Hanani M (2005) Satellite glial cells in sensory ganglia: from form to function. Brain Res Brain Res Rev 48:457–476.

Hanani M (2015) Role of satellite glial cells in gastrointestinal pain. Front Cell Neurosci 9:412.

Huang LY, Gu YP, Chen Y (2013) Communication between neuronal somata and satellite glial cells in sensory ganglia. Glia 61:1571–1581.

Huang TY, Belzer V, Hanani M (2010) Gap junctions in dorsal root ganglia: possible contribution to visceral pain. Eur J Pain 14:49 e1-e11.

Kawano H, Kimura-Kuroda J, Komuta Y, Yoshioka N, Li HP, Kawamura K, Li Y, Raisman G (2012) Role of the lesion scar in the response to damage and repair of the central nervous system. Cell Tissue Res 349:169–180.

Kim YS, Anderson M, Park K, Zheng Q, Agarwal A, Gong C, Saijilafu Young LA, He SQ, LaVinka PC, Zhou FQ, Bergles D, Hanani M, Guan Y, Spray DC, Dong XZ (2016) Coupled activation of primary sensory neurons contributes to chronic pain. Neuron 91:1085–1096.

Kirk T, Ahmed A, Rognoni E (2021) Fibroblast memory in development, homeostasis and disease. Cells 10:2840.

Li KC, Zhang FX, Li CL, Wang F, Yu MY, Zhong YQ, Zhang KH, Lu YJ, Wang Q, Ma XL, Yao JR, Wang JY, Lin LB, Han M, Zhang YQ, Kuner R, Xiao HS, Bao L, Gao X, Zhang X (2011) Follistatin-like 1 suppresses sensory afferent transmission by activating Na^+,K^+-ATPase. Neuron 69:974–987.

Liu P, Lu J, Cardoso WV, Vaziri C (2008) The SPARC-related factor SMOC-2 promotes growth factor-induced cyclin D1 expression and DNA synthesis via integrin-linked kinase. Mol Biol Cell 19:248–261.

Luo P, Shao J, Jiao Y, Yu W, Rong W (2018) CC chemokine ligand 2 (CCL2) enhances TTX-sensitive sodium channel activity of primary afferent neurons in the complete Freud adjuvant-induced inflammatory pain model. Acta Biochim Biophys Sin (Shanghai) 50:1219–1226.

Lynch MD, Watt FM (2018) Fibroblast heterogeneity: implications for human disease. J Clin Invest 128:26–35.

Nash GB, Buckley CD, Rainger GE (2004) The local physicochemical environment conditions the proinflammatory response of endothelial cells and thus modulates leukocyte recruitment. FEBS Lett 569:13–17.

Neves AF, Farias FH, de Magalhaes SF, Araldi D, Pagliusi M Jr, Tambeli CH, Sartori CR, Lotufo C, Parada CA (2020) Peripheral inflammatory hyperalgesia depends on P2X7 receptors in satellite glial cells. Front Physiol 11:473.

O'Shea TM, Burda JE, Sofroniew MV (2017) Cell biology of spinal cord injury and repair. J Clin Invest 127:3259–3270.

Ohara PT, Vit JP, Bhargava A, Romero M, Sundberg C, Charles AC, Jasmin L (2009) Gliopathic pain: when satellite glial cells go bad. Neuroscientist 15:450–463.

Oliveira ME, Santos FM, Bonifacio RP, Freitas MF, Martins DO, Chacur M (2017) Low level laser therapy alters satellite glial cell expression and reverses nociceptive behavior in rats with neuropathic pain. Photochem Photobiol Sci 16:547–554.

Pannese E, Ledda M, Arcidiacono G, Rigamonti L (1991) Clusters of nerve cell bodies enclosed within a common connective tissue envelope in the spinal ganglia of the lizard and rat. Cell Tissue Res 264:209–214.

Pannese E, Procacci P, Ledda M, Conte V (1993) The percentage of nerve cell bodies arranged in clusters decreases with age in the spinal ganglia of adult rabbits. Anat Embryol (Berl) 187:331–334.

Parsonage G, Falciani F, Burman A, Filer A, Ross E, Bofill M, Martin S, Salmon M, Buckley CD (2003) Global gene expression profiles in fibroblasts from synovial, skin and lymphoid tissue reveals distinct cytokine and chemokine expression patterns. Thromb Haemost 90:688–697.

Pozzi A, Yurchenco PD, Iozzo RV (2017) The nature and biology of basement membranes. Matrix Biol 57:1–11.

Previtali SC, Malaguti MC, Riva N, Scarlato M, Dacci P, Dina G, Triolo D, Porrello E, Lorenzetti I, Fazio R, Comi G, Bolino A, Quattrini A (2008) The extracellular matrix affects axonal regeneration in peripheral neuropathies. Neurology 71:322–331.

Rocnik EF, Liu P, Sato K, Walsh K, Vaziri C (2006) The novel SPARC family member SMOC-2 potentiates angiogenic growth factor activity. J Biol Chem 281:22855–22864.

Saikia P, Medeiros CS, Thangavadivel S, Wilson SE (2018) Basement membranes in the cornea and other organs that commonly develop fibrosis. Cell Tissue Res 374:439–453.

Scherer SS, Arroyo EJ (2002) Recent progress on the molecular organization of myelinated axons. J Peripher Nerv Syst 7:1–12.

Shin SM, Itson-Zoske B, Cai YS, Qiu CS, Pan B, Stucky CL, Hogan QH, Yu HW (2020) Satellite glial cells in sensory ganglia express functional

transient receptor potential ankyrin 1 that is sensitized in neuropathic and inflammatory pain. Mol Pain 16:1744806920925425.

Shvab A, Haase G, Ben-Shmuel A, Gavert N, Brabletz T, Dedhar S, Ben-Ze'ev A (2016) Induction of the intestinal stem cell signature gene SMOC-2 is required for L1-mediated colon cancer progression. Oncogene 35:549–557.

Singhmar P, Trinh RT, Ma J, Huo X, Peng B, Heijnen CJ, Kavelaars A (2020) The fibroblast-derived protein PI16 controls neuropathic pain. Proc Natl Acad Sci USA 117:5463–5471.

Song DD, Li Y, Tang D, Huang LY, Yuan YZ (2014) Neuron-glial communication mediated by TNF-α and glial activation in dorsal root ganglia in visceral inflammatory hypersensitivity. Am J Physiol Gastrointest Liver Physiol 306:G788–G795.

Sorge R, et al. (2012) Genetically determined P2X7 receptor pore formation regulates variability in chronic pain sensitivity. Nat Med 18:595–599.

Spray DC, Hanani M (2019) Gap junctions, pannexins and pain. Neurosci Lett 695:46–52.

Timpl R (1996) Macromolecular organization of basement membranes. Curr Opin Cell Biol 8:618–624.

Vannahme C, Gosling S, Paulsson M, Maurer P, Hartmann U (2003) Characterization of SMOC-2, a modular extracellular calcium-binding protein. Biochem J 373:805–814.

Wang K, Wang S, Chen Y, Wu D, Hu X, Lu Y, Wang L, Bao L, Li C, Zhang X (2021) Single-cell transcriptomic analysis of somatosensory neurons uncovers temporal development of neuropathic pain. Cell Res 31:904–918.

Xie AX, Madayag A, Minton SK, McCarthy KD, Malykhina AP (2020) Sensory satellite glial Gq-GPCR activation alleviates inflammatory pain via peripheral adenosine 1 receptor activation. Sci Rep 10:14181.

Yang L, Dong F, Yang Q, Yang PF, Wu R, Wu QF, Wu D, Li CL, Zhong YQ, Lu YJ, Cheng X, Xu FQ, Chen L, Bao L, Zhang X (2017) FGF13 selectively regulates heat nociception by interacting with $Na_v1.7$. Neuron 93:806–821.e9.

Yurchenco PD (2011) Basement membranes: cell scaffoldings and signaling platforms. Cold Spring Harb Perspect Biol 3:a004911.